

Recent advances in two-dimensional layered and non-layered materials hybrid heterostructures

Haixin Ma(马海鑫), Yanhui Xing(邢艳辉), Boyao Cui(崔博垚), Jun Han(韩军), Binghui Wang(王冰辉), and Zhongming Zeng(曾中明)

Citation: Chin. Phys. B, 2022, 31 (**10**): 108502. DOI: 10.1088/1674-1056/ac5c36
Journal homepage: http://cpb.iphy.ac.cn; http://iopscience.iop.org/cpb

What follows is a list of articles you may be interested in

Quantum oscillations in a hexagonal boron nitride-supported single crystalline InSb nanosheet

Li Zhang(张力), Dong Pan(潘东), Yuanjie Chen(陈元杰), Jianhua Zhao(赵建华), and Hongqi Xu(徐洪起)
Chin. Phys. B, 2022, 31 (**9**): 098507. DOI: 10.1088/1674-1056/ac7455

Bioinspired tactile perception platform with information encryption function

Zhi-Wen Shi(石智文), Zheng-Yu Ren(任征宇), Wei-Sheng Wang(王伟胜), Hui Xiao(肖惠), Yu-Heng Zeng(曾俞衡), and Li-Qiang Zhu(竺立强)
Chin. Phys. B, 2022, 31 (**9**): 098506. DOI: 10.1088/1674-1056/ac7a15

Thermionic electron emission in the 1D edge-to-edge limit

Tongyao Zhang(张桐耀), Hanwen Wang(王汉文), Xiuxin Xia(夏秀鑫), Chengbing Qin(秦成兵), and Xiaoxi Li(李小茜)
Chin. Phys. B, 2022, 31 (**5**): 058504. DOI: 10.1088/1674-1056/ac464d

Electrostatic gating of solid-ion-conductor on InSe flakes and InSe/h-BN heterostructures

Zhang Zhou(周璋), Liangmei Wu(吴良妹), Jiancui Chen(陈建翠), Jiajun Ma(马佳俊), Yuan Huang(黄元), Chengmin Shen(申承民), Lihong Bao(鲍丽宏), and Hong-Jun Gao(高鸿钧)
Chin. Phys. B, 2020, 29 (**11**): 118501. DOI: 10.1088/1674-1056/aba60a

Photovoltaic effects in reconfigurable heterostructured black phosphorus transistors

Siqi Hu(胡思奇), Ruijuan Tian(田睿娟), Xiaoguang Luo(罗小光), Rui Yin(殷瑞), Yingchun Cheng(程迎春), Jianlin Zhao(赵建林), Xiaomu Wang(王肖沐), Xuetao Gan(甘雪涛)
Chin. Phys. B, 2018, 27 (**12**): 128502. DOI: 10.1088/1674-1056/27/12/128502

REVIEW

Recent advances in two-dimensional layered and non-layered materials hybrid heterostructures

Haixin Ma(马海鑫)[1], Yanhui Xing(邢艳辉)[1,†], Boyao Cui(崔博垚)[1], Jun Han(韩军)[1], Binghui Wang(王冰辉)[1], and Zhongming Zeng(曾中明)[2,3]

[1] *Key Laboratory of Opto-electronics Technology, Ministry of Education, College of Microelectronics, Beijing University of Technology, Beijing* 100124, *China*

[2] *Key Laboratory of Nanodevices and Applications, Suzhou Institute of Nano-tech and Nano-bionics, Chinese Academy of Sciences, Suzhou* 215123, *China*

[3] *Nanchang Nano-Devices and Technologies Division, Suzhou Institute of Nano-Tech and Nano-Bionics, Chinese Academy of Sciences, Nanchang* 330200, *China*

(Received 22 November 2021; revised manuscript received 6 February 2022; accepted manuscript online 10 March 2022)

With the development of Moore's law, the future trend of devices will inevitably be shrinking and integration to further achieve size reduction. The emergence of new two-dimensional non-layered materials (2DNLMs) not only enriches the 2D material family to meet future development, but also stimulates the global enthusiasm for basic research and application technologies in the 2D field. Van der Waals (vdW) heterostructures, in which two-dimensional layered materials (2DLMs) are physically stacked layer by layer, can also occur between 2DLMs and 2DNLMs hybrid heterostructures, providing an alternative platform for nanoelectronics and optoelectronic applications. Here, we outline the recent developments of 2DLMs/2DNLMs hybrid heterostructures, with particular emphasis on major advances in synthetic methods and applications. And the categories and crystal structures of 2DLMs and 2DNLMs are also shown. We highlight some promising applications of the heterostructures in electronics, optoelectronics, and catalysis. Finally, we provide conclusions and future prospects in the 2D materials field.

Keywords: 2D layered materials, 2D non-layered materials, van der Waals heterostructure, applications

PACS: 85.60.–q, 81.07.–b, 85.30.–z **DOI:** 10.1088/1674-1056/ac5c36

1. Introduction

Since the emergence of graphene in 2004, two-dimensional (2D) materials represented by graphene have developed rapidly. New 2D layered materials (2DLMs) have sprung up and numerous works have been urgently studied, including graphene, black phosphorus (BP), transition metal dichalcogenides (TMDCs), and so on. Due to the unique crystal structure and chemical properties, the 2D materials structure has shown great application prospects in photoelectricity, sensing, catalysis, energy storage, biological imaging, and magnetic recording.[1–5] Many advantages compared with their bulk counterparts are shown in the following part. (i) The charge carriers, heat, and photons transport are strongly confined in a 2D plane, resulting in unusual physical phenomena such as two-dimensional electron gas (2DEG) and the quantum Hall effect.[6] And 2D electronic confinement has produced many unique electrical properties, making it suitable for electronic device and basic condensed matter research.[7–9] (ii) The band gap of many 2D materials can be adjusted by changing the thickness. Moreover, the ultra-thin thickness can shorten the migration distance of carriers and reduce the recombination of photogenerated carriers, which is suitable for high-gain optical devices with adjustable band gap.[10] (iii) 2D geometric structure has good compatibility with the current thin film manufacturing technology. And strong in-plane covalent bonds and ultra-thin thickness give them great flexibility and mechanical strength, which is suitable for fabricating flexible devices.[11] (iv) The ultra-high specific surface area make them suitable for research on surface catalysis-related applications.[12] Therefore, 2D materials have been extensively studied over the past few years to build high-performance and functional devices because of these advantages.

Nowadays, heterogeneous structure building has been proven to be effective in achieving the function and adjusting the performance.[13,14] Van der Waals (vdW) heterostructure created by stacking different 2DLMs with highly distinct electronic states have shown interesting physical properties. However, due to many inherent limitations of 2DLMs, such as the limited number of 2DLMs, high in-plane symmetry and chemically inert surfaces, it is difficult to meet full-wavelength detection, high-performance polarized light detection, and high-active surface requirements applications. The emergence of 2D non-layered materials (2DNLMs) with three-dimensional (3D) chemically bonded crystal structure is necessary, which not only greatly expands the scope of the 2D materials but

†Corresponding author. E-mail: xingyanhui@bjut.edu.cn

© 2022 Chinese Physical Society and IOP Publishing Ltd

also exhibits a series of interesting properties beyond the scope of 2DLMs. The surface atoms of the 2DNLMs are unsaturated, providing an additional degree of freedom to tailor the properties of materials and heterostructures built from them. And the absence of free dangling bonds on the surfaces of 2DLMs allow them to be easily integrated with other semiconductors materials to form high-quality heterojunctions beyond the limitation of lattice matching. The combination of 2DLMs and 3D materials into heterojunctions has been studied, which showed extraordinary applications in many aspects. However, due to size constraints, the device can not be further reduced and integrated. Therefore, more and more studies focused on 2DLMs/2DNLMs heterojunction devices.[15,16]

Although there are many reviews providing a general overview of 2D materials and applications, there has been no specific summary article focusing on hybrid heterostructures based on 2DLMs and 2DNLMs.[12,17–19] Here, we outline the recent progress of 2DLMs/2DNLMs heterojunction. The categories and crystal structures of 2DLMs and 2DNLMs are also shown. And we emphasize some promising applications of the heterostructures in electronics, optoelectronics, and catalysis. Finally, we provide conclusions and future prospects.

2. Materials category and crystal structure

In recent years, new types of 2D atomic crystal materials have been discovered. High-quality 2D atomic crystal materials play an important role in exploring new physical phenomena and further expanding their applications in high-performance electronic devices, optoelectronic devices and others. Despite the differences in the crystal structure and intrinsic properties for different 2D materials, they can all be classified into two types: 2DLMs and 2DNLMs. The fundamental point of distinction between 2DLMs and 2DNLMs lies in the forces between out-of-plane atoms. For 2DLMs, the in-plane atoms are connected by strong chemical bonds within 2D plane, while the layers are stacked together relying on weak vdW forces. Non-layered stacked 2D materials, formed by chemical bonding in the 3D direction. There is no obvious natural delamination inside the crystal. The crystal thickness can be thinned to atomic level dimensions and presented at 2D planes with lateral dimensions by breaking the chemical bonds in the vertical direction inside the crystal. In this part, a brief introduction about category and crystal structure of these widely explored 2D nanomaterials will be given.

2.1. 2D layered materials

Figure 1 lists the extensively studied members in the 2D layered materials family. We all know that stability is a key issue for 2D materials. Therefore, we have classified it according to the difference in stability. For a single-layer film, the green area materials are constant in the ambient environment (room temperature in the air). The orange area materials are stable in the air, but the gray area materials are stable only in an inert atmosphere. In addition to these materials, there are some such as hydroxides, perovskite-type, which are only retained in the material preparation stage. Except for the results of atomic force microscope (AFM), no further research information has been reported. The properties and crystal structures of several representative layered 2D materials are highlighted in this part.

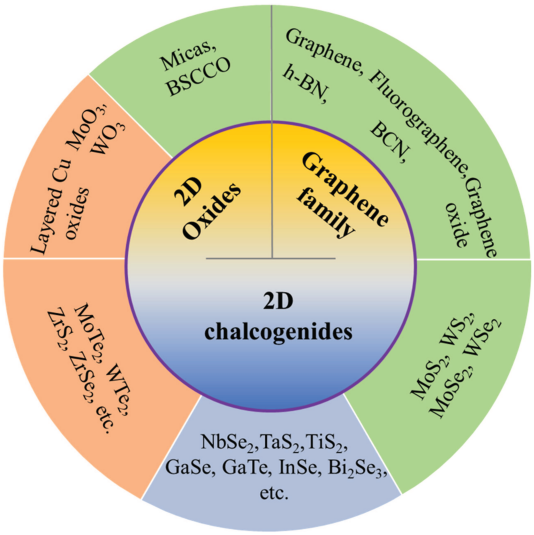


Fig. 1. Layered 2D materials library.

Graphene is a single atomic layer of carbon atoms arranged in a hexagonal lattice (honeycomb), with a thickness of about 0.335 nm (Fig. 2(a)).[20] The carbon atoms of graphene are connected by sp^2 hybrid bonds with a bond length of 0.142 nm and π bonds in the vertical plane, and this special structure allows graphene to exhibit many excellent properties.[21] The room temperature mobility reaches 2.5×10^5 $cm^2\cdot V^{-1}\cdot s^{-1}$, and the low temperature (4 K) mobility is nearly 6×10^6 $cm^2\cdot V^{-1}\cdot s^{-1}$. The thermal conductivity is the highest of all materials, about 2000 $W\cdot m^{-1}\cdot K^{-1}$ to 5300 $W\cdot m^{-1}\cdot K^{-1}$, and can withstand a current density 1×10^6 times higher than that of copper.[21] However, the zero-bandgap structure of graphene makes its optical absorption not strong, and the electron–hole pairs are extremely easy to recombine, leading to the poor responsiveness of the photodetector.

Boron nitride (BN) is a crystal composed of boron and nitrogen atoms. Hexagonal boron nitride (h-BN) has a layered graphite-like phase, and its crystal structure is shown in Fig. 2(b). The structure and properties of h-BN are very similar to graphite, and it is a white solid, commonly known as "white graphene". H-BN is sp^2 hybridized and the distance between two neighboring atoms is about 0.25 nm.[22] And

the h-BN has good mechanical properties, thermodynamic, chemically stable, high temperature resistance, and so on, so it is widely studied in the field of catalysis. And h-BN as a carrier, a variety of inorganic materials for composite has also achieved more research results.[23] The boron–carbon–nitrogen (BCN) layered material can be regarded as a mixture of graphite and BN. The difference in C doping has an impact on the electronic structure. And similar to graphite, the BCN layered structure can also generate nanotubes. And the BCN nanotube is considered to be an effective blue and violet light emitter.[24]

BP has a similar 2D layered structure to graphene and is the third allotrope of phosphorus monomers besides white and red phosphorus, whose orthorhombic crystal structure is shown in Fig. 2(c).[25] The distance between adjacent layers is 0.5 nm. BP is a natural p-type semiconductor. The vector of free electrons is constant, so it is a direct band gap no matter how many layers are peeled off, and the forbidden band width is between 0.3 eV–1.5 eV. The shear stress is small in the x-direction because of the anisotropy, which results in the effective mass of the electrons being only 0.1 m_0–0.15 m_0 and a very high electron mobility.[26]

The chemical formula of TMDCs can be expressed as MX_2, where M represents the transition metal elements Mo, W, Ta, Nb, V, Re; X represents the sulfur group elements S, Se, Te. MX_2 consists of two layers of sulfur group atoms (X) and a layer of transition metal atoms (M) in between, forming an "X–M–X sandwich" layered structure. Each layer is a hexagonal lattice, which is stacked into a bulk material by vdW forces perpendicular to the in-plane. At present, more than 40 different TMDCs 2D atomic crystal materials can be formed by various combinations of sulfur group elements and transition metal elements. Among the TMDCs atomic crystal materials, MoS_2 has been studied the most. The crystal structure is shown in Fig. 2(d), with the sulfur atoms in the upper and lower layers and metal atoms in the middle layer.[27] The interlayer spacing is 0.65 nm. When MoS_2 is thinned from bulk material to monolayer, the electron leap mode changes from non-vertical to vertical leap, and the electron energy band structure changes from indirect to direct band gap, and the photoelectric conversion efficiency improves. The forbidden band width also increases as the number of layers decreases. For example, the gap bands of the blocks MoS_2 and WS_2 are 1.19 eV and 1.35 eV, respectively, and in the case of a single layer, the gap bands increase to 1.9 eV and 2.05 eV. In addition, TMDCs also have a unique feature of forming different polycrystalline forms. Take MoS_2 as an example, it has five different crystal structures crystallized, namely 2H, 1T, 1T′, 1T‴, and 3R.[28] Among them, 2H MoS_2 is the most stable, and other metastable crystal structures will be transformed into 2H MoS_2 under certain conditions.

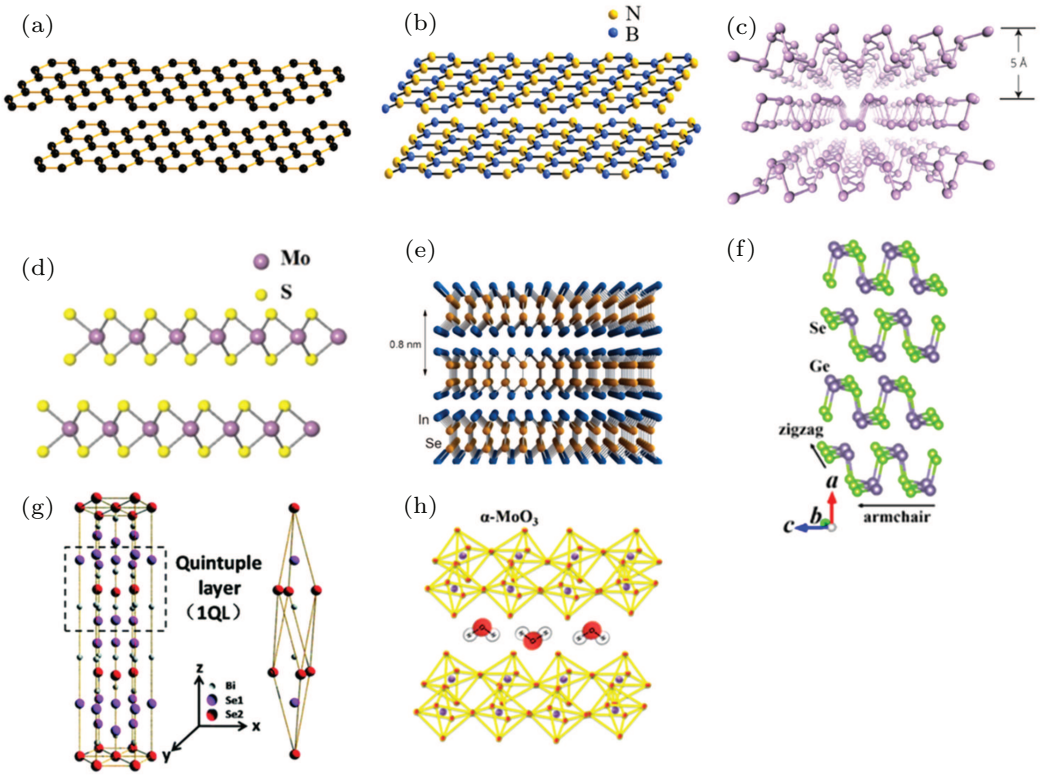


Fig. 2. Crystal structures of the represented 2D layered materials. (a) Graphene, (b) h-BN, (c) BP, (d) MoS_2, (e) InSe, (f) GeSe, (g) Bi_2Se_3, (h) MoO_3. Figures reproduced with permission from Ref. [25] (panel (c)) ©2014 Nature Publishing Group; Ref. [27] (panel (d)) ©2017 WILEY-VCH Verlag GmbH & Co. KGaA, Weinheim; Ref. [1] (panel (e)) ©2018 American Chemical Society; Ref. [10] (panel (f)) ©2020 IOP Publishing Ltd Printed in the UK; Ref. [34] (panel (g)) ©2015 The Royal Society of Chemistry; Ref. [35] (panel (h)) ©2016 Nature Publishing Group.

Main group metal sulfides are another form of layered metal sulfide, which include group III–VI and group IV–VI layered semiconductors, expressed by the general formula MX, M = Ga, In (group III), Ge, Sn, Pb (group IV) and X = S, Se, Te.[29] The most representative InSe material of III–VI semiconductor materials, it has a unique Se–In–In–Se structure with interlayer vdW force connection at an interlayer distance of $d \approx 0.8$ nm (Fig. 2(e)). Each layer has a hexagonal structure with D_{3h} symmetry. In the range of 20 K–300 K, the Hall mobility can reach 2×10^3 cm$^2 \cdot$V$^{-1} \cdot$s^{-1}, which is higher than that of transition metal sulfides used for FETs widely.[30] IV–VI layered semiconductors have a distorted NaCl-type structure. Take GeSe as an example, the crystal structure is shown in Fig. 2(f).[10] The bulk GeSe is a layered material with an orthogonal structure, each unit cell has eight atoms and two puckered layers, and each atomic layer is bound together by vdW forces.[31]

Topological insulator (TIs) is a new quantum state of matter with peculiar quantum effects, in which the body becomes like an insulator showing insulating properties, while the surface resembles a conductor showing metallic properties.[32,33] Bi_2Se_3 is a representative material for TIs. Its rhombic crystal structure is displayed in Fig. 2(g) with a space point group of $R\text{-}\bar{3}m/D_{3d}^5$ and a lattice constant of 4.1 Å in the a and b axes and 28.6 Å in the c axis. From the structural diagram of Bi_2Se_3 crystal, it can be found that its smallest structural unit is composed of every five atomic layers (quintuple layer, QL), and each quintuple layer is arranged in the order of Se–Bi–Se–Bi–Se.[34] The atoms between the layers of Bi_2Se_3 are bonded by ionic covalent bonds, while the layers are connected by weak vdW forces.

Metal trioxide has a layered structure, and the general formula is MO_3 (M = Mo, Ta, W, *etc*.). Figure 2(h) gives an example of MoO_3 crystal structure.[35,36] The phase stability and crystal structures of MoO_3 are determined by the position of the basic building block MoO_6 octahedron. Among the three phases of α, β, and h, the orthorhombic phase α-MoO_3 is the most stable, consisting of twisted MoO_6 octahedral units bound by covalent bonds along the a [100] and c [001] directions and by vdW forces along the b [010] direction.[37]

2.2. 2D non-layered materials

Nowadays, although the research of 2DLMs has achieved great success, in order to expand the types and quantities of 2D materials, it is necessary to study 2DNLMs with more excellent functional materials and 3D chemically bonded crystal structure. 2DNLMs can possess simultaneously the characteristics of 2D structures and bulk structures, thus exhibiting many interesting properties.[38] The main categories of 2DNLMs include metals, metal chalcogenides, metal oxides, topological crystalline insulators, group III–V semiconductors and organic–inorganic chalcogenides. Table 1 briefly summarizes the types crystal structures, synthesis methods, applications and representative performance of main 2DNLMs. The thickness of 2DNLMs is about 0.4 nm–300 nm, and some of them are thicker than 2DLMs. As can be seen from Table 1, as with 2DLMs, 2DNLMs are also mainly used in electronic and optoelectronic devices. However, the addition of 2DNLMs can provide a platform for adjusting the disadvantages of the previous 2DLMs devices, and it also opens up new ideas for the development of 2D material devices in the future.

With different crystalline properties and 2D planar structures, 2DNLMs have shown excellent properties in many applications. For example, group III–V semiconductor GaN nanosheets exhibit significant changes in electronic and optical properties due to surface and size effects.[39] First, 2D GaN nanosheets show enlarged bandgap, blue-shifted photoluminescence (PL) emission peak, thus being expected to be an excellent candidate for nano-electronics and optoelectronics.[12] Second, due to the lack of inversion and mirror symmetry, the 2D GaN nanosheets in the wurtzite phase exhibit inherent polarization along the out-of-plane direction, resulting in strong quantum confinement Stark effect and piezoelectric effect.[40] Third, due to the unsaturated dangling bonds-induced highly active surface and the unique electronic structure-induced rapid carrier transport and separation, the 2DNLMs GaN exhibits high-efficiency catalytic ability and enhanced energy storage performance.[41,42] Take another example, Ag is a metal with a face-centered cubic atomic structure, its physical and chemical properties are relatively stable, with good thermal and electrical conductivity, soft in quality, and rich in ductility. Its reflectivity is extremely high, reaching more than 99%. The 2DNLMs Ag nanoplates were synthesized by a two-step process for the controlled growth.[43] With the advantages of precise size control and high reproducibility, this two-step process can easily produce Ag nanoplates with high aspect ratios (up to 400 or more), providing an excellent platform for catalytic preparation. The plasmon band of NL2DM Ag can tune from the visible to the infrared spectrum, making them ideal candidates for biomedical application such as photothermal cancer. Moreover, as a member of 2DNLMs, single crystal β-Ga_2O_3 has a unique monoclinic structure with a highly anisotropy lattice constants. β-Ga_2O_3can be also exfoliated into nano-layers along the (100) direction, while maintaining the excellent characteristics of single crystals.[44–46] Other non-layered materials were prepared by mechanical peeling method including goethite (a-FeOOH), galena (PbS), calcite ($CaCO_3$), and so on. The specific synthesis methods and applications of some representative materials will be discussed in detail in the following sections.

Table 1. Summary of 2D non-layered materials.

Categories	Materials/crystal structures	Synthetic methods	Thickness/size	Applications	Performances	References
Metal	Ag/cubic	seeded growth process	<10 nm/~ 4 μm	–	–	[43]
	Pd/hexagonal	magnetron sputtering method	16 nm/4.5 mm	sensors (H_2)	currents change about 840% and 13,100%. (Pd/p-Si, Pd/n-Si)	[47]
	Mg/hexagonal close-packed	cryogenic exfoliation	~ 20 nm/~ 500 nm	–	Excellent plasmonic behavior	[48]
	Rh/hexagonal	solvothermal synthesis	~ 0.4 nm/500 nm–600 nm	catalyst	$>99.9\%$ conversion within 4 h at near room temperature (30°) under low H_2 pressure (1.0 MPa)	[49]
	Co/orthorhombic	ligand-confined growth	~ 0.84/ ~ 400 nm–500 nm	sensors (CO_2)	overpotential=0.24 V, selectivity=90.1%	[50]
Metal oxides	WO_3/monoclinic, TiO_2/anatase	spray pyrolysis technique	–	photocatalyst	an efficient photocatalytic ability (salicylic acid) under UV illumination	[51]
	In_2O_3/cubic	hydrothermal process	37.5 nm/5–8 μm	sensors (ethanol)	superior repeatability and reliable selectivity, LOD: ~ 0.4 ppm (260 °)	[52]
	ZnO/wurtzite	hydrothermal method	–	photocatalyst	degradation of methylene blue enhanced by 500%	[53]
	MoO_2/monoclinic	high temperature solid synthesis method	~ 1.4 nm/~ 10 μm	–	SERS signals enhance by 10^4	[54]
	α-Fe_2O_3/hexagonal	water dissolvable template-based synthesis	1 nm/~ 5 μm	catalyst	tafel slope: 56 mV·dec^{-1}, high stability in acidic media	[55]
	CoO/wurtzite	ionic layer epitaxy	2.8 nm/>cm	catalyst	current density: 10 mA·cm^{-2}, tafel slope=85 mA	[56]
	β-Ga_2O_3/monoclinic	thermal oxidation	9 nm/> 20 μm	photodetector	254 nm, $V_{ds}=10$ V; $R=3.3$ A/W, EQE=1600%, $D^*=4\times10^{12}$ Jones, $\tau_{rise}=30$ ms, $\tau_{delay}=60$ ms	[57]
Metal chalcogenides	PbS/cubic	VdWE	5 nm–35 nm/ ~ 4 μm	photodetector	800 nm, $V_{ds}=0.1$ V; $R=1621$ A/W, $G=2512$, $D^*=1.7\times10^{11}$ Jones, $\tau_{rise}=0.3$ s, $\tau_{delay}=0.3$ s	[58]
	PbTe/cubic	VdWE	~ 7 nm/~ 10 μm	photodetector	1550 nm, $V_{ds}=0.04$ V; $R=3847$ A/W, $\tau_{rise}=2.71$ s, $\tau_{delay}=4.4$ s	[59]
	In_2S_3/cubic	CVD	25 nm/~ 50 μm	self-power photodetector	405 nm, $V_{ds}=2$ V; $R=740$ mA/W, $G=780$, $D^*=1.5\times10^{10}$ Jones, $\tau_{rise}=9$ ms, $\tau_{delay}=10$ ms	[60]
	Cr_2S_3/rhombohedral	ambient pressure CVD	~ 1.78 nm/200 μm	FET	on/off ratio: over 10^3	[61]
	ZnSe/zinc-blende	solvothermal synthesis	~ 0.89–0.92 nm/ ~ 500 nm	photocatalytic water splitting	IPCE: 42.5%, photocurrent density: 2.14 mA/cm^2, $\tau=18.1$ s	[62]
TCIS	SnTe/cubic	VdWE	~ 3.6 nm/$\sim$ 8μm	photodetector	980 nm, $V_{ds}=0.5$ V; $R=698$ mA/W, EQE=88.5%, $D^*=3.8\times10^8$ Jones, $\tau_{rise}=1.45$ s, $\tau_{delay}=0.6$ s	[11]
	$Pb_{1-x}Sn_xTe$/cubic	CVD	40 nm/20 μm	–	–	[63]
III–V semiconductors	GaN/wurtzite	surface-confined nitridation reaction (CVD)	4.1 nm/50 μm	FET	electronic mobility: 160 cm^2·V^{-1}·s^{-1}, on/off ratio: $\sim 10^6$	[64]
	GaAs/zinc-blende	chemical exfoliation method	18 nm/–	photodetector	532 nm, $V_{ds}=25$ V; $R=677$ A/W, $D^*=8.6\times10^{12}$ Jones, $\tau_{rise}=70$ ms, $\tau_{delay}=52$ ms	[65]
Organic-inorganic perovskites	$CH_3NH_3PbBr(I,Cl)_3$/tetragonal	liquid-phase growth	~ 8 nm/hundreds of micrometers	photodetector	450 nm, $V_{ds}=5$ V; $R=126$ A/W, on/off ratio: $\sim 10^4$, $\tau_{rise}=5$ μs, $\tau_{delay}=4.1$ μs	[66]
Others	ZnSb/orthorhombic	CVD	~ 132–140 nm/10 μm	photodetector	1550 nm, $V_{ds}=0.5$ V; $R=89.2$ A/W, $D^*=1.7\times10^{10}$ Jones, EQE=7140%, $\tau_{rise}=9.6$ ms, $\tau_{delay}=90$ ms	[67]
	δ-FeOOH/feroxyhyte	wet chemistry approach	~ 1.9 nm/~ 50 μm	electrolysis water splitting	high water splitting performance for HER and OER	[68]
	γ–CuI/triangular, hexagonal	facile PVD	~ 1 nm/5 μm	FET	low resistivity: ~ 0.3 Ω·cm	[69]
	$CuGaSe_2$/tetragonal	cation exchange method	~ 45 nm/~ 328 nm	photodetector	532 nm, $V_{ds}=1$ V; $\tau_{rise}=50$ s, $\tau_{delay}=50$ s	[70]

CVD: chemical vapor deposition; VdWE: Van der Waals epitaxy; PVD: physical vapor deposition; G: photo-gain; IPCE: photon-to-current conversion efficiency; HER: hydrogen evolution reaction; OER: oxygen evolution reaction; SERS: surface-enhanced Raman spectroscopy; LOD: corresponding detection limits; EQE: external quantum efficiency; R: responsivity; D^*: detectivity; G: photo-gain.

3. Hybrid heterostructures and synthesis methods

Currently, vdW heterojunctions prepared by combining the advantages of 2DLMs and 2DNLMs are constantly appearing in the public view. Compared with traditional heterojunction, the advantage of vdW heterojunctions of 2D atomic crystal materials lies in the convenience of modular combination. Depending on the building structure of the heterojunctions, they can be divided into vertical heterostructures and lateral heterostructures. In this section, based on different preparation methods, we respectively describe the different properties and applications about the devices of the two heterojunction structures. In the future, it is possible to create a variety of new devices by using reasonable device design and microscopic analysis methods to determine the key position parameters.[71]

3.1. Lateral heterojunctions (in-plane)

As early as 2015, it was reported for the heterojunctions of in-plane 2DLMs and 2DNLMs combining their advantages. The performance of the corresponding devices is improved. Feng *et al.* discovered that InSe nanosheets can be easily transformed into $CuInSe_2$ thin film and naturally form in-plane InSe/$CuInSe_2$ p–n heterojunction by using a simple solid-state reaction method with elemental copper at a temperature of 300 °C.[72] Specifically, the mechanically exfoliated InSe is first transferred to the SiO_2/Si substrate by dry transfer method. Then, half of the sheet area was masked by the Cu film using thermal evaporation. A simple cleaning step of 5-min submersion in 3-M aqueous $FeCl_3$ removes the residual Cu on the nanosheets after annealing. As a result, the seamless 2D InSe/$CuInSe_2$ lateral heterojunction is spontaneously constructed. Lateral InSe/$CuInSe_2$ p–n diode based on photodetectors show a responsivity of 4.2 A/W. And the heterojunction photovoltaic device improves conversion efficiency to 3.5%. This work provides a facile method for fabricating 2D in-plane 2DLMs/2DNLMs heterojunctions, and offers new opportunities for high-performance photodetectors. But the thermal evaporation reaction has poor repeatability, making it difficult to ensure the uniformity of the $CuInSe_2$ film. In recent years, pulsed laser deposition (PLD) has been used to fabricate 2D materials due to their outstanding advantages, such as quantitative stoichiometry, digital control of film thickness, and high growth rates, making it easy to maintain consistent synthesis conditions.[73] Ji *et al.* designed laterally self-assembled $CuInSe_2$/InSe heterojunctions by PLD.[74] Concretely, symmetric Cu–Au electrodes are firstly patterned onto mica substrates. When depositing InSe using PLD, In and Se atoms can reassemble Cu atoms from Cu electrodes and finally form lateral heterojunctions. The dark current can be effectively suppressed to cause a high switching ratio. And the photocurrent of the heterojunction photodetector increased to about 4 times higher than that of the pure InSe device. Moreover, from the comparison of the performance of these two optoelectronic devices, the performance of the device prepared by the PLD method is better than that of the device prepared by the thermal evaporation method, which is directly related to the preparation method of the materials. Zhang *et al.* also developed *in-situ* preparation of in-plane In_2Se_3/$CuInSe_2$ heterojunctions using PLD technology.[75] The photocurrent, R, and EQE of the 2DLMs/2DNLMs heterojunction photodetector improve by ~ 1 order of magnitude as compared to a pristine In_2Se_3 device. And the response speed of the heterojunction photodetector is 8.3 ms which is only half of the pure In_2Se_3 device. For PbS/graphene heterostructures, PbS nanoplates will selectively grow along the edges of graphene nanosheets due to the presence of highly active unsaturated carbon atoms by vapor epitaxy technology. The photodetectors based on PbS/graphene heterostructures achieved an ultrahigh photoresponsivity of 10^7 A/W and photoconductive gain of 10^8.[76] And PbS nanoplates are also in contact with TMDCs MoS_2 edges through strong chemical hybridization. Its heterojunction photodetectors improved detectivity to 3×10^{13} Jones and response speed to 7.8 ms.[77]

Most recently, another direct writing approach enables precise nanometer-scale heterojunction with a high accuracy. Laser-based surface oxidation of the top few layers has been achieved to protect the crystal surface from degradation over time.[78] Following this success, Mukherjee *et al.* enhanced the effect of local laser heating to break the atomic bonds by increasing the visible probe irradiation power and formed stable In–O bonds completely by oxidation, resulting in the construction of lateral In_2Se_3/In_2O_3 heterojunctions (Fig. 3(a)).[16] The elemental distribution on laser-written boxes and its surrounding area are shown in Fig. 3(b), revealing the homogenous in-plane distribution of elements. The 2D overlayer mapping (Fig. 3(c)) further confirms the presence of detectable quantities and homogeneous distribution of In_2O_3 at the illumination area. Furthermore, a type-II band alignment heterojunction was deduced (Fig. 3(d)), which is beneficial for photodetectors. The atomically thin In_2O_3 layers enhanced 2 orders of magnitude of conductivity and mobility, and the metal–semiconductor interfaces transformed from Schottky to ohmic contact. The heterojunction photodetector demonstrates a stable and repetitive photo-response (Fig. 3(e)). Compared with the original In_2Se_3 photodetector, the responsivity and the detectivity of the heterojunction photodetector has been improved by an order of magnitude, in addition to extending the detection range of visible light (Fig. 3(f)). In addition, Ren *et al.* showed an another route to fabricate lateral Sb_2Se_3/β-In_2Se_3 p–n heterojunctions via an *in-situ* melt-quenching method.[79] The highest photocurrent density obtained in the heterojunction (90% Sb_2Se_3–10% β-In_2Se_3) device was 283 times higher than that of pure Sb_2Se_3 device. The Sb_2Se_3/β-In_2Se_3 p–n heterojunctions also shown the interesting photocatalytic activity. These methods reveal a promising technological prospect for all-2D lateral heterojunction construction.

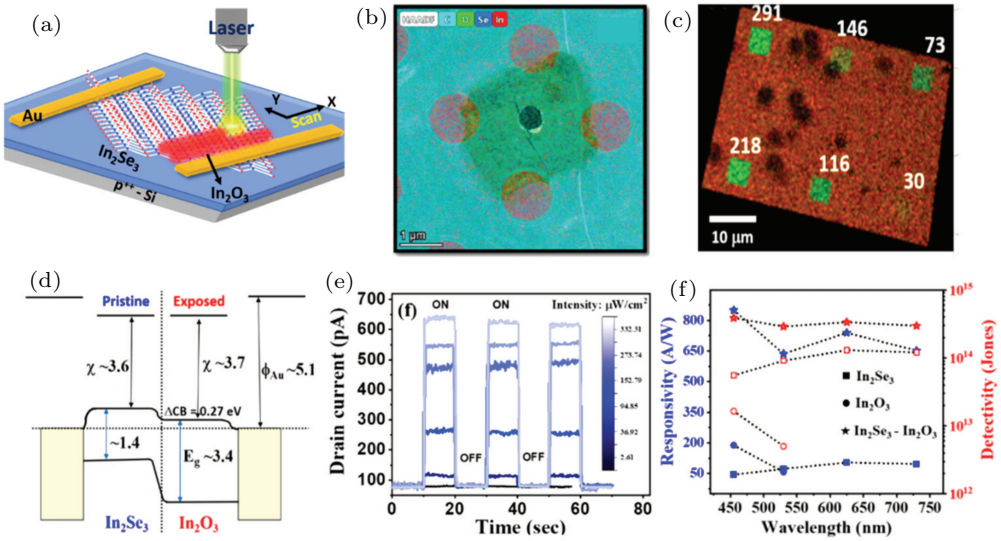


Fig. 3. (a) A schematic illustration of the In_2Se_3/In_2O_3 heterojunction fabrication. (b) Elemental distribution on laser-written boxes and its surrounding area for 72.85 mW/μm^2. (c) 2D image of the In_2O_3 overlayer on an In_2Se_3 background under different laser powers. The green-colored boxes indicate the laser-written area. (d) Band diagram of the heterojunction device under equilibrium condition. (e) Time response (at 60-V gate bias) of the heterojunction for different illumination intensities. (f) Wave-length-dependent photo-responsivity (solid symbols) and photo-detectivity (open symbols) data for all three devices. Figures reproduced with permission from Ref. [16], ©2020 American Chemical Society.

3.2. Vertical heterojunction (out-plane)

A large number of out-of-plane 2DLMs/2DNLMs heterostructures were reported by the manual stacking method up to now.[80–83] One of the main advantages of the manual stacking method is preserving the pristine electronic properties of bulk materials. 2DNLMs is limited by isotropic covalent bonds in all three dimensions, thus making it difficult to produce 2DNLMs by simple mechanical exfoliation methods with corresponding bulk crystal delamination. Recently, non-van der Waals hematite (the lamellar specularite variety, a-Fe_2O_3) has been successfully exfoliated into 'hematene', N-dimethylformamide (DMF) along the (001) layer orientation.[84] Inspired by the exfoliation of layered hematite along the non-layer orientation, many non-layered materials were found to possess perfect cleavage planes with anisotropic in-plane and out-of-plane bonding, which will contribute to the generation of atomically smooth surfaces along the cleavage orientations. Exfoliated nanosheets have been applied to various electronic and optoelectronic devices, such as metal oxide semiconductor field effect transistors (MOSFETs), metal–semiconductor field-effect transistors (MESFETs) and solar-blind photodetectors as well as self-driven photodetectors[83,85–87] and even catalysis.[88] The β-Ga_2O_3 nanosheets can be easily constructed with common 2D materials such as graphene, BN, and TMDCs to achieve a variety of vertical heterostructures.[81–83,86,89] An ultrahigh deep-UV sensitivity phototransistor using graphene and mechanical exfoliated β-Ga_2O_3 was demonstrated, the photo-to-dark current ratio were raised by 6 orders of magnitude under the optimal gate bias.[80] The fabrication process for graphene-gated metal–semiconductor phototransistor based on β-Ga_2O_3 flake is shown in Fig. 4(a). The exfoliated β-Ga_2O_3 has a thickness of ∼ 280 nm (red line in Fig. 4(c)). The Raman spectra (graphene (bottom) and β-Ga_2O_3 (top), in Fig. 4(b)) obtained from the overlapped junction area indicates that phonon positions of the exfoliated β-Ga_2O_3 are consistent with those measured for highly crystalline β-Ga_2O_3 in previous reports.[45,87] However, the interface of the heterostructure may be contaminated by the chemical residue during the transfer process, which could make a large impact in the quality of the heterojunction devices. Meanwhile, the size, the thickness, and the shape of the produced ultrathin 2D nanomaterials are difficult to control because the exfoliation process is operated manually by hands, which lack the precision, controllability or repeatability. And the production rate is quite slow, which make it difficult to realize the demands for various practical applications, high yield and large-scale production.

By comparing with mechanical peeling method, direct synthesis methods with bottom-up strategy such as chemical vapor deposition (CVD) and physical vapor deposition (PVD), have been proved to be powerful tools in preparing large-area 2D materials and their heterostructures.[11,38,90,91] However, the traditional bottom-up method can not be used to synthesize 2DNLMs due to the lack of a drive force to break the symmetry of bulk crystals and promoting the growth of anisotropy. Optimized CVD methods urgently need to be developed, including van der Waals epitaxy (vdWE) growth, space-confined CVD, and self-limited epitaxial growth. Recently, vdWE growth method exhibits great potential in realizing highly anisotropic growth of 2DNLMs. Making use of 2D layered materials as the vdWE substrates, many 2D non-layered materials were successfully synthesized, such as Te, PdTe, SnTe, CdS, $Pb_{1-x}Sn_xSe$, and PbS nanoplates.[58,59,63,92–94] The lateral size, morphology, and layer number of the materials

can be adjusted by the growth parameters, such as growth temperature, rate of gas flow, and volume of precursors. Whereafter, some out-of-plane 2DLMs/2DNLMs heterostructures such as MoS_2/CdS, MoS_2/PbSe, graphene/PbS, and so on, have been fabricated by this method.[76,95–97] Specifically, Zheng and co-workers synthesized 10-nm–60-nm-thick CdS nanoplates on few-layer MoS_2 substrate, though the lattice mismatch between hexagonal CdS and MoS_2 was calculated to be 32% (Figs. 5(a) and 5(b)). The response speed of MoS_2/CdS vertical heterostructure photodetectors are far faster than single-layer MoS_2-based photodetectors (over 10 s *versus* 100 ms). The responsivity is increased by over 50 times (70.8 $mA{\cdot}W^{-1}$ *versus* 3.91 $A{\cdot}W^{-1}$) under 610-nm illumination. This study also indicates that vdW epitaxy allows formation of high quality vertical heterostructure consisting of two 2D materials with such large lattice mismatch because of the weak vdW interaction at the interface. He *et al.* synthesized $Pb_{1-x}Sn_xSe$ nanoplates with 10-nm–70-nm-thick on few-layer BN substrate. And PbS nanoplates/graphene junctions and PbSe/MoS_2 heterostructures with edge contact were also fabricated.[76,77] The microscopic behavior of the PbS nanoplates/graphene heterostructure is shown in Fig. 5(c). Selected-area-electron diffraction pattern shown in Fig. 5(d) clearly confirmed the edge contact way. The photodetector based on PbS/graphene junction exhibited an ultrahigh photo-gain ($\approx 10^8$), responsivity (10^6 A/W) and a fast response speed ($\tau_{rise} = 24$ ms, $\tau_{decay} = 59$ ms). In addition, PbSe quantum dots[96] and 2D PbS nanoplates arrays[77] on MoS_2 nanosheets, 2D CdTe nanosheets with wurtzite crystal structure,[98] and 2D hexagonal CdSe nanoplates[99] on mica substrate were also successfully obtained. It can be foreseen that bottom-up optimized CVD methods will be a very promising method to manufacture 2D non-layered materials and their heterojunctions.

Owing to the synthesis difficulties for some 2D materials, the heterojunctions based on these materials have not been fully fabricated, and the potential new electronic and optoelectronic properties are still unclear. Recently, Huang and co-workers reports a high responsivity and fast ultraviolet (365 nm) to short-wavelength-infrared (1550 nm) photodetector based on Cd_3As_2/MoS_2 heterojunction.[15] The photodetector exhibits a short response time in broad spectra region. The excellent performance of the Cd_3As_2/MoS_2 photodetector marks that the PVD method has been extended to Dirac semi-metal materials and their heterojunctions. And sputtering technology can also prepare 2DNLMs and their heterojunctions, such as Ga_2O_3/graphene,[100] VO_2/$MoTe_2$,[101] VO_2/MoS_2.[102] In 2020, through the liquid metal printing technology combined with a surface-confined nitridation reaction method, Zhang and co-workers firstly fabricated large area and very thin (2.55 nm–4.62 nm) 2D GaN flakes, which break through the difficulty of preparing high-quality non-layered 2D GaN crystals.[103] And the photoelectric properties and related photogenerated carrier dynamic mechanisms of the MoS_2/GaN vdWs heterostructure were investigated. In addition, Lu and co-workers firstly fabricated a graphene/In_2S_3 heterostructure via PLD method in 2018 and systematically explored its transport behaviors and optoelectronic characteristics.[104] Next year, the same group used the same method to prepare a high-performance graphene/In_2S_3 heterojunction photodetector.[105] The detection range is between 400 nm–1200 nm, and it has extremely fast response speed (40 μs) and super high responsivity (4.53×10^4 $A{\cdot}W^{-1}$).

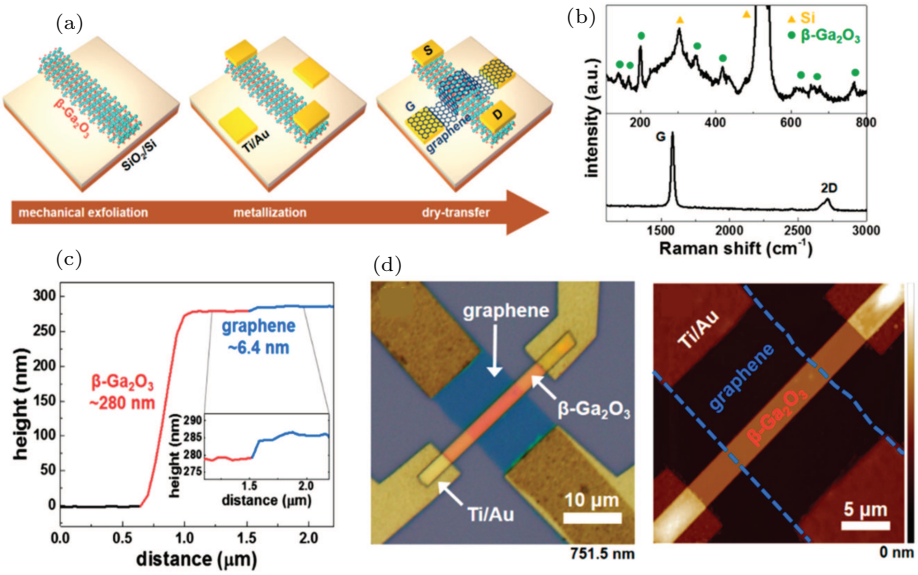


Fig. 4. (a) Schematic diagram of the fabrication process for graphene-gated metal–semiconductor phototransistor based on β-Ga_2O_3 flake. (b) Raman spectra for β-Ga_2O_3(top) and graphene (bottom) in the junction region. (c) The corresponding height profile of β-Ga_2O_3 (red) and graphene (blue) used in the device. (d) Optical microscope image and atomic force microscopy (AFM) image of the fabricated phototransistor. Reproduced with permission from Ref. [80], ©2019 American Chemical Society.

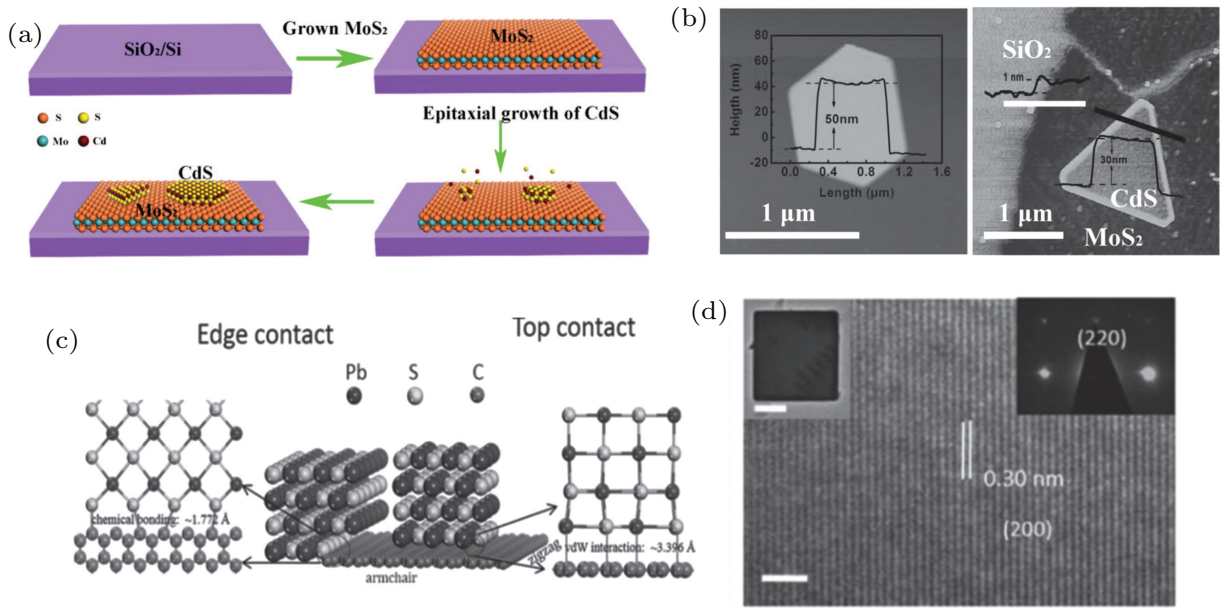


Fig. 5. (a) Schematic illustration of one-step epitaxial growth of CdS/MoS_2 heterostructures. (b) AFM image and associated height profile of a hexagonal CdS (left) and AFM phase image of the heterostructure with associated height profiles (right). (c) Schematic diagram of microscopic behavior of PbS nanoplates–graphene heterostructure. (d) High-resolution transmission electron microscopy (HRTEM) shows distinct crystal fringes of PbS nanoplate. Selected area electron diffraction (SAED) in upper right inset presents a well-defined square pattern, confirming the highly single crystalline of PbS nanoplate with orientation ⟨110⟩ along edge of graphene. Reproduced with permission from Ref. [95] (panels (a) and (b)), Ref. [76] (panels (c) and (d)) ©2016 WILY-VCH Verlag GmbH & Co. KGaA, Weinheim (panels (a) and (b)), ©2016 WILY-VCH Verlag GmbH & Co. KGaA, Weinheim (panels (c) and (d)).

4. Applications

2DLMs materials possess compelling physical properties and promising application prospects. 2DNLMs show additional superior surface activity and stronger quantum confinement effect than 2DLMs. The combination of the 2DLMs and 2DNLMs further broadens applications of the 2D materials and might overcome intrinsic restrictions. In this part, we outline the latest advances on the representative applications of the 2DLMs/2DNLMs heterojunctions, highlighting electronics, optoelectronics, and catalysts field.

4.1. Electronic devices

Among the applications of 2D materials in microelectronic devices, 2D field-effect transistors (FETs) have attracted tremendous attention. Due to their excellent electrical characteristics, such as ultra-low power consumption, high current switching ratio, and large carrier mobility. Recent years, more and more researchers focused on 2DLMs/2DNLMs heterojunctions electronic devices. Various devices including junction field-effect transistor (JFETs), metal–insulator–semiconductor field-effect transistors (MISFETs) and MESFETs, and so on have been designed. By integration of graphene and n-type β-Ga_2O_3, a high breakdown electric field in β-Ga_2O_3/graphene vertical barristor heterostructure was reported (see Fig. 6(a)).[81] Off-state I_d–V_{ds} electrical characterization of the β-Ga_2O_3/graphene vertical devices were performed (see Fig. 6(b)). A record breakdown field is 5.2 MV/cm, exceeding the previously reported values on other materials FETs (see Fig. 6(c)). The RF performance of Ga_2O_3/graphene and β-Ga_2O_3/BP heterostructure MOSFETs has been proposed and investigated.[106] Kim and co-worker firstly integrated an E-mode with a D-mode MESFET based on graphene/β-Ga_2O_3 heterostructure (see Fig. 7(a)).[85] Both E-/D-modes β-Ga_2O_3 MESFETs exhibit excellent electrical characteristics, with a high on/off current ratio of 10^7 and ideality factors of ~ 1.5 (see Fig. 7(b)). The MESFET operated in the E-mode with a positive threshold voltage of $+0.25$ V and a low subthreshold swing of 68.9 mV/dec, which are better than that of a single-gate D-mode FET. And monolithic integration of E-/D-mode quasi-2D β-Ga_2O_3 FETs enabled the first presentation of a low-dimensional β-Ga_2O_3 logic circuit (see Fig. 7(c)). The logic inverter showed a good inversion functionality and a well-matched operating range from 0 V to 1.4 V. The voltage gain can be improved by optimizing the device layout of E- and D-mode transistors. And the gain value is high when compared with an AlGaN/GaN HEMT-based direct-coupled FET logic inverter. And an n-channel D-mode WSe_2/β-Ga_2O_3 JFET was also fabricated.[82] The p-WSe_2/n-Ga_2O_3 heterostructure exhibits excellent rectifying behaviors, with a high on/off current ratio of 10^8, a low subthreshold swing of 133 mV/dec and a three-terminal breakdown voltage of $+144$ V. And the gate leakage current main-

tained a significantly low level of approximately 10^{-8} mA/mm under negative gate bias. Recently, Choi *et al.* reported an ambipolar channel p-TMD/n-Ga_2O_3 JFETs (see Fig. 8(a)).[107] The ambipolar channel transistor means that n-type β-Ga_2O_3 and p-type TMD separately play as a channel for JFETs with each type of carriers. Current–voltage characteristics based on p-$MoTe_2$/n-Ga_2O_3 JFETs show a high on/off current ratio of $\approx 10^8$ along with ideality factor of 2.4 and a very small leakage current of only a few tens fA (see Fig. 8(c)). For more extended applications, the p-TMD/n-Ga_2O_3 JFETs architecture was put to high-speed photo-switching operation (see Fig. 8(d)). For p-WSe_2 channel JFETs, the switching frequency and response time is about 16 kHz and 30 μs under red illuminations. And for p-$MoTe_2$ channel JFETs, these two values further up to 29 kHz and down to 17 μs under NIR illuminations (see Fig. 8(f)). The photo-switching speed of the p-TMD JFET is the fastest among 2D-based FETs. The high switching speed of JFET is due to the rapid transfer of photocarriers in the TMD channel.

In addition to semiconductor properties, the two-dimensional materials also have insulator properties and are used in electronic devices. For example, the boron nitride can be used as an alternative dielectric material, in which the thermal conductivity of 50 $W{\cdot}m^{-1}{\cdot}K^{-1}$ is higher than the other dielectric materials, such as SiO_2 (1.4 $W{\cdot}m^{-1}{\cdot}K^{-1}$) and Al_2O_3 (35 $W{\cdot}m^{-1}{\cdot}K^{-1}$). The BN integrated with β-Ga_2O_3 to fabricate a BN/β-Ga_2O_3 heterostructure MISFET, showed a lower gate leakage current.[83] Moreover, a large on/off ratio of $\sim 10^7$ and a small subthreshold swing of 175 mV/dec could be achieved. Up to now, some other 2DLMs/2DNLMs heterojunctions devices have also been reported, such as γ-CuI/WS_2(WSe_2),[69] MoS_2/ZnO,[108,109] ZrO_2/MoS_2,[110] $CrBr_3$/GaN,[40] and so on.

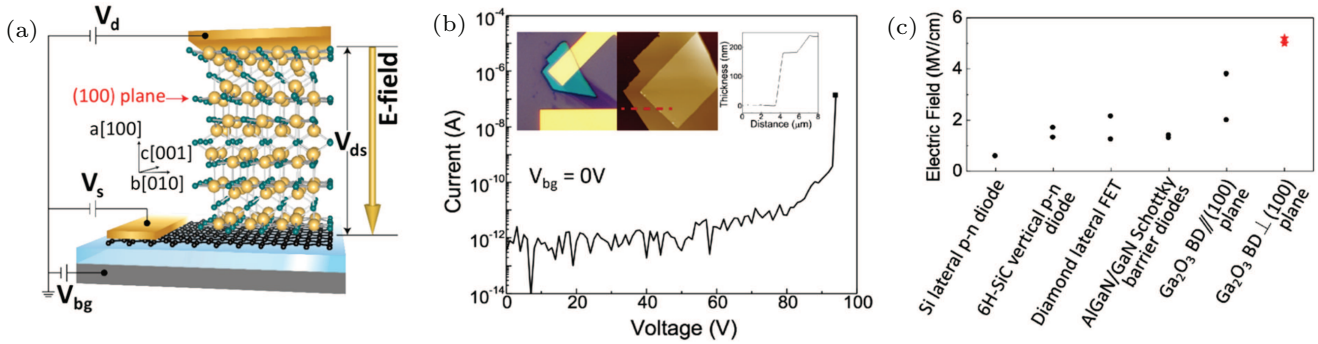


Fig. 6. (a) Schematic diagram of a β-Ga_2O_3/graphene vertical device. (b) The off-state breakdown voltage of the barristor device. (c) Comparisons of breakdown electric fields measured on various semiconductor materials for power device applications. Reproduced with permission from Ref. [81], Published by AIP Publishing.

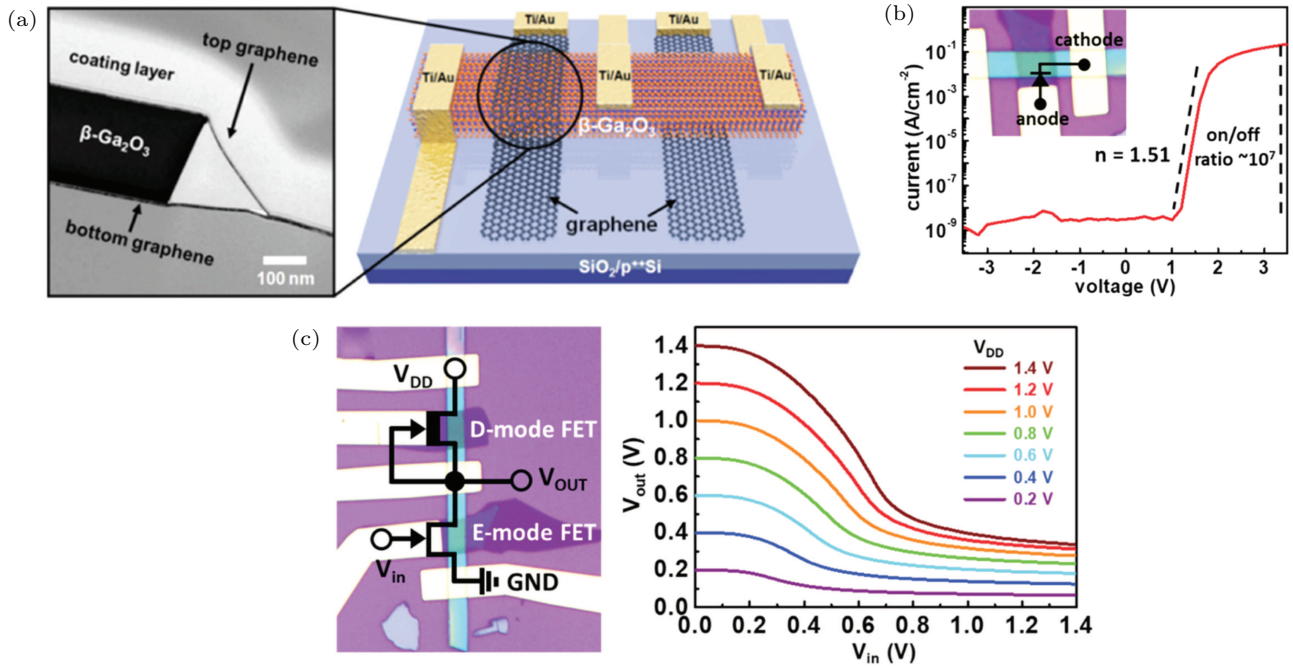


Fig. 7. (a) Schematic diagram of the series of the integrated E-/D-mode graphene/β-Ga_2O_3 MESFETs. (b) The rectifying *I*–*V* curve of a graphene/β-Ga_2O_3 Schottky junction. (c) The logic inverter fabricated by E-/D-mode MESFETs and voltage transfer characteristics of the inverter at different V_{DD}. Reproduced with permission from Ref. [85], ©2020 American Chemical Society.

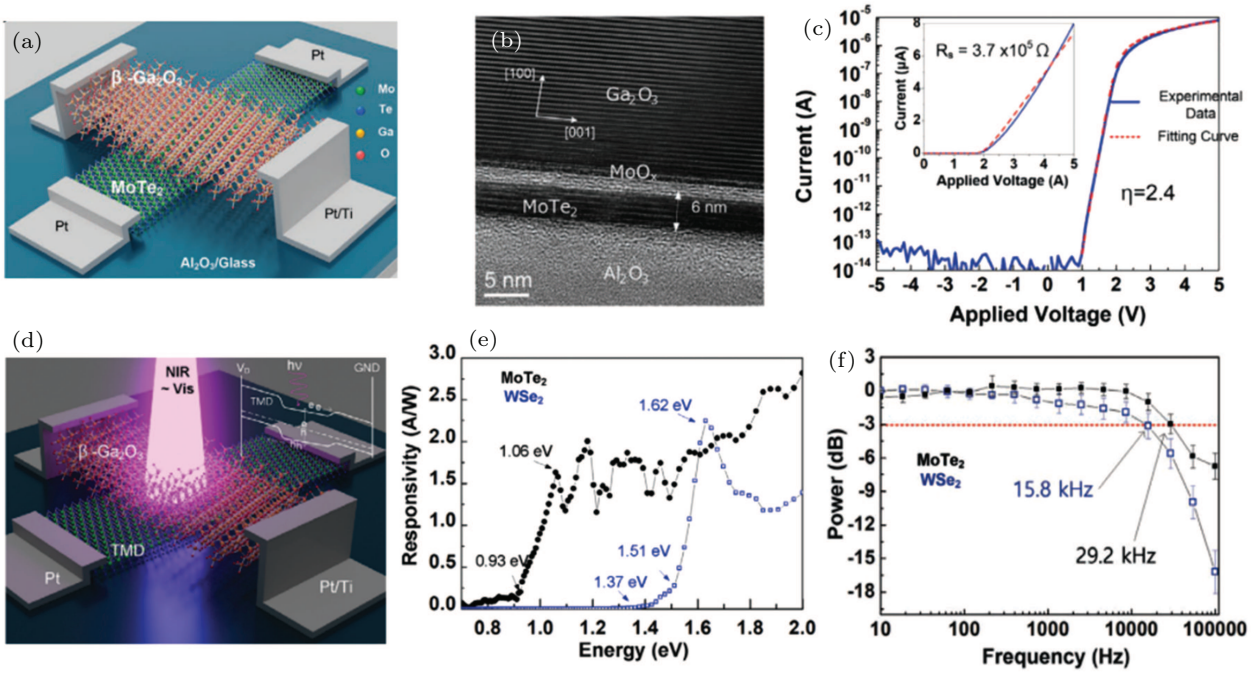


Fig. 8. (a) Schematic diagram of p-$MoTe_2$/n-Ga_2O_3 junction device architecture. (b) Cross section TEM images of the junction structure. (c) The rectifying *I*–*V* curve of the device. (d) Schematic diagram of the photo-sensing measurement. (e) The responsivity–photon energy plots of $MoTe_2$ and WSe_2 channels. (f) Bandwidth measured for p-$MoTe_2$ and p-WSe_2 channel JFETs. Reproduced with permission from Ref. [107], ©2021 Wiley-VCH GmbH.

4.2. Optoelectronic devices

Photodetector is mainly used in monitoring, chemical-biological analysis, communication, health care, energy harvesting, and so on. An effective photodetector must meet four vital features including high photoresponsivity, low noise, fast response speed, and multiwavelength detection in complex application systems. 2D materials have provided new opportunities for the effective photodetector owing to their tunable work function, strong light–matter coupling, and ultrafast carrier dynamics. Since the addition of 2DNLMs in the 2D material family, photodetectors based on 2D materials can achieve visible-blind or even solar-blind detection. And the integration of 2DLMs with 2DNLMs opens up new ideas for improving the performance of photodetectors. For example, Lu and co-workers reported a vdW heterostructure composed of In_2S_3 and graphene via the dry transfer method (Fig. 9(a)).[104] The photodetector based on In_2S_3/graphene heterostructure exhibits excellent optical responsive performance due to the synergy of photoconductive and photogating effects. And the device's photo-response can be effectively modulated by its gate voltage. At gate voltage of 0 V, an ultrahigh responsivity of 795 A/W and an external quantum efficiency of 2440% can be achieved under the illumination of 405-nm light (Fig. 9(c)). As the gate voltage increases to 60 V, these two parameters can be further increased to 8570 A/W and 26200% (Fig. 9(d)), much higher than previously reported values for In_2S_3-based detectors. Inspired by the pioneer work done, a hybrid Ga_2O_3/graphene solar-blind photodetector was fabricated by sputtering Ga_2O_3 on graphene.[100] The photodetector shows long-term environmental stability and outstanding mechanical flexibility without any encapsulation. The obtained *R*, EQE, and D^* of the device are 2.75 A/W, 1.1×10^4%, and 8.4×10^{13} Jones, respectively, which could be ascribed to the efficient photogenerated electron–hole pair separation by the strong built-in field near the 2DLMs/2DNLMs interface. In order to further enhance the device performance, a larger potential barrier is highly required. Researchers turned to construct p–n junctions other than Schottky barrier junctions by replacing graphene with other 2D semiconductors. MoS_2 possesses overwhelming advantages, including good chemical stability, high theoretical phonon limited mobility, and considerable thermal stability, which are especially suitable for light detection. In 2020, a 2D MoS_2/GaN p–n junction photodetector was fabricated (Fig. 10(a)).[103] Under a 532-nm light illumination, the *R*, EQE, D^* of the photodetector are as high as 328 A/W, 764%, and 2×10^{11} Jones, respectively (Fig. 10(b)). The photo-response time of the MoS_2/GaN heterojunction photodetector is much faster than that of the pristine MoS_2 photodetector. The device also exhibits an outstanding UV light response with a high photoresponsivity of 27.1 A/W upon 365-nm light illumination. In addition, the detection range of the 2DLMs/2DNLMs heterojunction device has also been expanded. A Cd_3As_2/MoS_2 heterojunction photodetector with a quite high responsivity of 2.7×10^3 A/W is fabricated.[15]

The photodetector exhibits a fast response in broad spectra region from ultraviolet (365 nm) to short-wavelength-infrared (1550 nm). A self-powered operation mode photodetector is achieved by the $VO_2/MoTe_2$ heterostructure.[101] The p–n junction exhibits from mid-wavelength infrared to long-wavelength infrared detection with a response time of 17 μs. The photodetectors based on Cd_3As_2/MoS_2 and $VO_2/MoTe_2$ not only exhibit high performance, but also greatly expands the detection range. Nowadays, a series of other photodetectors based on 2DLMs/2DNLMs have been successfully fabricated, such as the following listed listed in Table 2: $PbSe/MoS_2$,[96] $CuInSe_2/InSe$,[72,74] $CuInSe_2/In_2Se_3$,[75] $In_2O_3/InSe$,[78] In_2O_3/In_2Se_3,[16] In_2S_3/graphene,[104,105] PbS/graphene,[76] PbS/MoS_2,[77] CdS/MoS_2,[95] Cd_3As_2/MoS_2,[15] VO_2/MoS_2,[102] $VO_2/MoTe_2$,[101] VO_2/GaSe,[111] MoO_3/MoS_2,[112] GaN/MoS_2,[103] Ga_2O_3/graphene,[80,100,113] $CH_3NH_3PbBr_3$/graphene,[114] and so on. These studies have led to continuous breakthroughs in the performance parameters of the optoelectronic device. Development of the 2DLMs/2DNLMs heterojunction device provides numerous platforms for both fundamental research and technological applications.

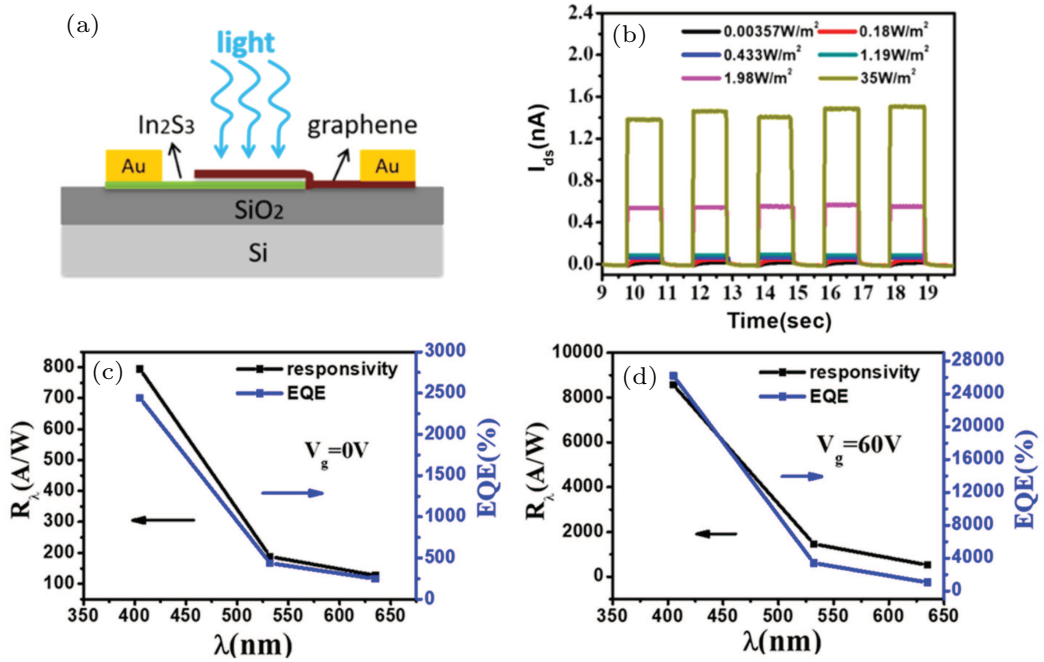


Fig. 9. (a) Schematic illustration of the In_2S_3/graphene heterostructure. (b) Time dependence of I_{ds} under a 405-nm laser with different light intensities. (c) and (d) Responsivity (black) and EQE (blue) as a function of wavelength at a gate voltage of 0 V and 60 V, respectively. Reproduced with permission from Ref. [104], ©2018 American Chemical Society.

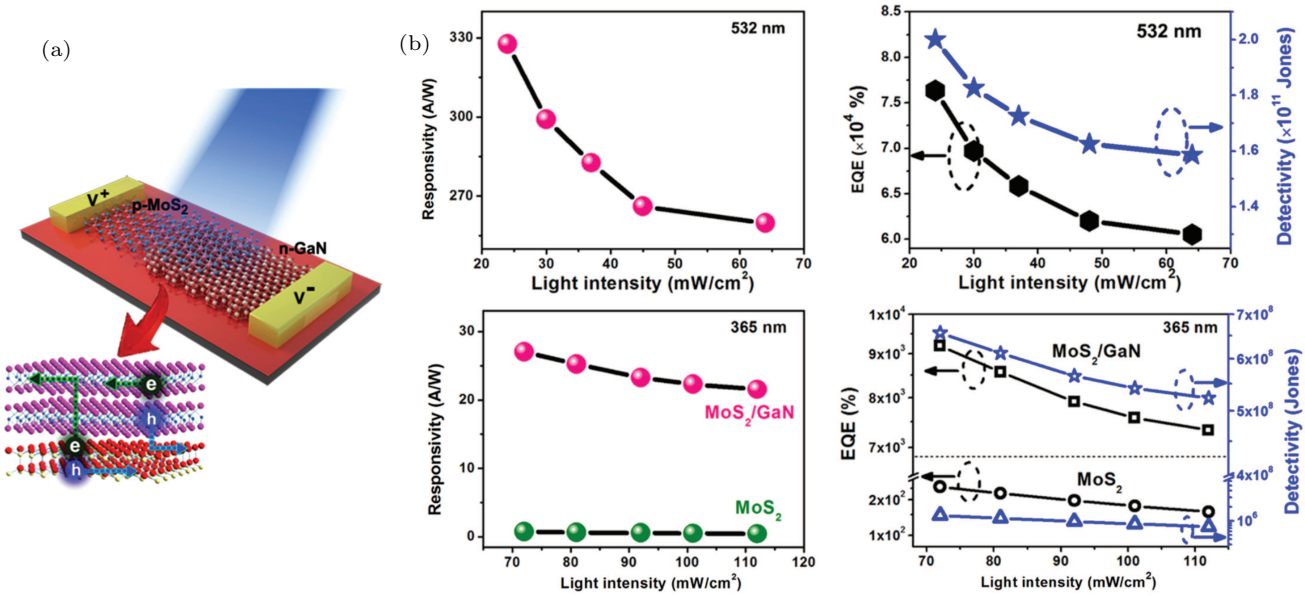


Fig. 10. (a) Schematic diagram of the electron−hole pair generation and transfer at the heterostructure interface under illumination. (b) The plot of the corresponding *R*, EQE, and D^* *versus* light intensity under 532-nm and 365-nm light illuminations. Reproduced with permission from Ref. [103], ©2020 American Chemical Society.

Table 2. Summary of other 2DLMs/2DNLMs heterojunction photodetectors.

Device	Laser λ (nm)	Responsivity (A/W)	Rise/fall time (ms)	Detectivity (Jones)
$PbSe/MoS_2$[96]	> 1200	–	150/430	–
$CuInSe_2/In_2Se_3$[75]	532	20.1	8.3	–
$CuInSe_2/InSe$[74]	405	–	300/600	–
$In_2O_3/InSe$[78]	NIR to UV	–	–	–
In_2S_3/graphene[105]	405	4.53×10^4	0.04	3.02×10^{11}
PbS/graphene[76]	800	2.5×10^6	24/59	–
PbS/MoS_2[77]	800	4.5×10^4	7.8	3×10^{13}
CdS/MoS_2[95]	610	3.91	100	–
Cd_3As_2/MoS_2[15]	365–1550	2.7×10^3	0.043/0.065	–
VO_2/MoS_2[102]	500–800	–	–	–
$VO_2/MoTe_2$[101]	MWIR to LWIR	0.22	0.017/0.039	3×10^{10}
$VO_2/GaSe$[103]	405	0.3581	0.041	2.14×10^{11}
MoO_3/MoS_2[112]	532	527	900/700	–

4.3. Catalysts

By using various materials and structures, the photocatalytic reaction triggered by solar energy can be divided into water splitting, CO_2 reduction, pollutant removal, organic synthesis reactions, and so on. Since the photocatalytic efficiency of most photocatalysts is still low, people urgently need new materials with excellent photocatalytic activity. 2D materials have attracted great interest in recent years due to their super-high specific surface area, short electron diffusion path, and improved structural stability. The 2DNLMs have been proven to have high-efficiency catalytic capabilities for various catalytic processes.[115,116] The unsaturated dangling bonds on the 2DNLMs surface provide numerous active surface sites for catalysis, facilitating the activation of the reaction substrates and expanding the scope of application. Recently, the improvement of photo-excited charge separation efficiency and reasonable band offsets design of 2DLMs/2DNLMs vdW heterojunctions make photocatalytic activity enhance. Yang and co-workers reported a AlN/BP heterojunction photocatalyst for water splitting.[117] The direct bandgap characteristic in the AlN/BP heterostructure is a type-II band alignment, which is more beneficial to improving the photocatalytic efficiency compared to the pristine BP. This group also found the enhanced photocatalytic mechanisms for the hybrid AlN/MX_2 ($MX_2 = MoSe_2$, WS_2, and WSe_2) nanocomposites by density-functional-theory calculations.[118]

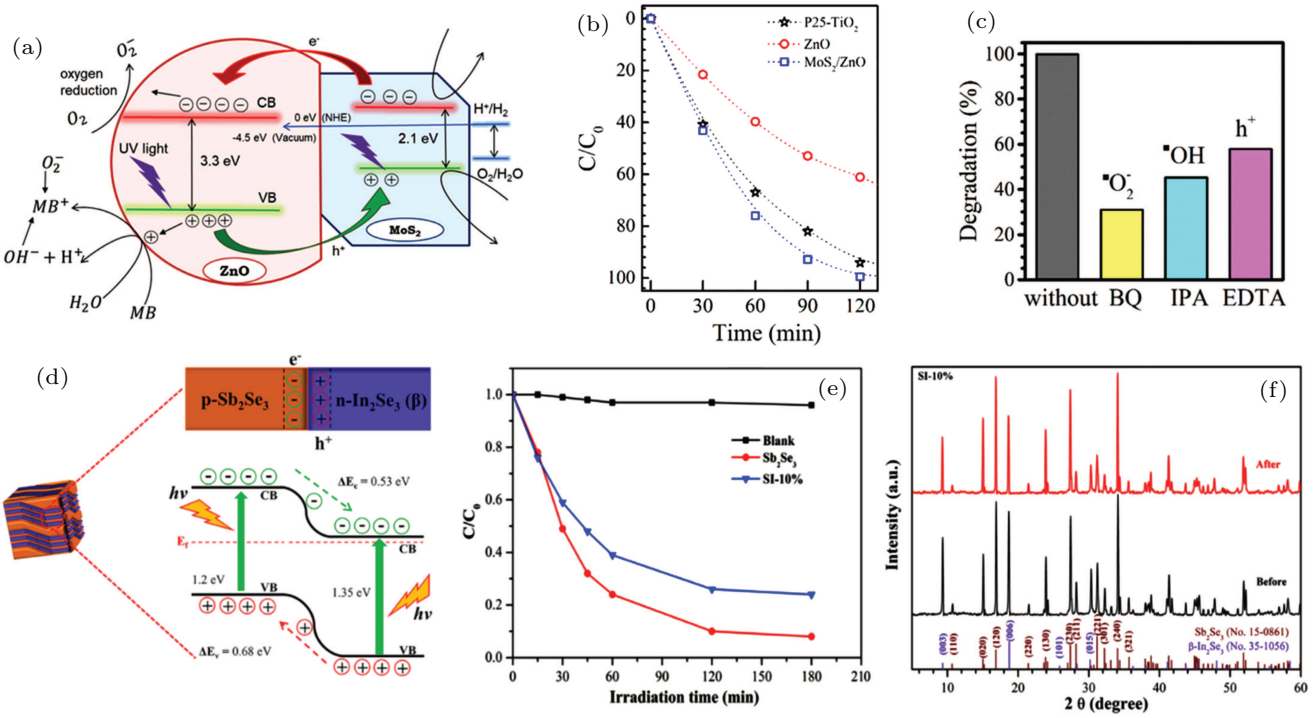


Fig. 11. (a) Schematic representation of photocatalytic mechanism. (b) Photocatalytic degradation curve. (c) Scavenger test results. (d) Schematic illustration of photoinduced electron–hole separation and transfer in Sb_2Se_3/β-In_2Se_3 heterojunction. (e) Degradation profiles of methyl orange solution under white light illumination. (f) The XRD patterns of sample before and after the photocatalytic reactions. Reproduced with permission from Ref. [121] (panels (a) and (c)), ©2019 Elsevier B.V. All rights reserved. Reproduced with permission from Ref. [79] (panels (d) and (f)), ©2020 Elsevier Ltd and Techna Group S.r.l. All rights reserved.

Since it was discovered that boron-doped ZnO nanoparticles loaded on MoS_2 nanosheets have enhanced photocatalytic activity to remove pollutants.[119] Then Rahimi *et al.* found that MoS_2 nanosheets could enhance the sunlight-induced photocatalytic activity rate of ZnO by 74%[120] (Fig. 11(a)). And a 40% enhancement in photocatalytic degradation was observed in a type-II MoS_2/ZnO heterostructure[121] (Figs. 11(b) and 11(c)). Ren *et al.* reported a series of Sb_2Se_3/β-In_2Se_3 heterojunctions with different contents of β-In_2Se_3[17] (Fig. 11(d)). The optimized composites (90% Sb_2Se_3–10% β-In_2Se_3) exhibited the highest photocurrent density that was about 283 times higher than that of pure Sb_2Se_3. Moreover, due to the facilitated separation and transport of photogenerated charge carriers, the photocatalytic activity was enhanced (Fig. 11(e)). After 180 min of illumination, 76% of methyl orange dye could be decomposed. And the Sb_2Se_3/β-In_2Se_3 composite was stable after the photocatalytic reactions (Fig. 11(f)).

Catalytic oxidation of CO is another catalytic method and is considered to be a promising method to solve the problem of environmental pollution. It is reported that the 2D SnO_2 sheet with 40% surface atom occupancy rate shows better CO catalytic performance than bulk SnO_2 and SnO_2 nanoparticles, which is manifested in the reduced apparent activation energy (59.2 kJ·mol^{-1}) and reduced full-conversion temperature. And the catalytic reaction at 250 °C for 54 hours did not deactivate, which confirmed the excellent structural stability and stable CO conversion ability.[12] At present, other 2DLMs/2DNLMs heterojunction studies have been reported on catalysis applications, such as CdS_ySe_{1-y}/MoS_2,[122] WO_3/WS_2-MoS_2,[123] MoS_2/ZnS,[124] and so on. According to these results, it indicates that the unique properties between 2D materials heterojunctions can produce more extraordinary devices in the field.

5. Conclusions and perspectives

Two-dimensional materials, with both layered and non-layered structures, have been a rising new star in the low-dimensional material field. The vdW heterostructures, where 2D materials are physically stacked layer by layer without the chemical bonding and interfacial lattice matching effects, have provided a flexible platform in nanoscale device applications. And the concept of vdW heterojunctions can also be extended between 2DLMs and 2DNLMs. In this review, we systematically review the classification and crystal structure of 2DLMs and 2DNLMs. The synthesis method and device application of 2DLMs and 2DNLMs heterostructure are emphasized. Depending on the building structure of the heterojunctions, they can be divided into vertical heterostructures and lateral heterostructures. The research of heterojunction fabrication technology revolves around these two parts. In addition, we highlight the applications of 2DLMs/2DNLMs heterojunctions in electronics, optoelectronics, and catalysts field. The vdW heterostructure between 2D materials has been studied in depth for decades. The various hybrid heterostructures introduced in this review have proven the widespread use of the vdW 2DLMs/2DNLMs heterojunction combination. However, the integration of 2DLMs and 2DNLMs based on vdW heterostructure is still in its infancy. Studying these heterojunctions and exploring their basic theories will be the next urgent topic. At the same time, the basic research and practical device applications of 2DLMs/2DNLMs heterostructures also face many challenges and opportunities, which are briefly described as follows.

(i) Develop practical application capabilities

The practical application capabilities of 2DLMs need to be developed. This is required not only a large area of controllable equipment but also the subsequent material transfer. Moreover, 2DLMs doping for adjusting energy level needs to be achieved not using the traditional semiconductor doping method of replacing atoms in a 3D material. In addition, many applications need to grow a layer of dielectric material on active semiconductor materials. 2DLMs are almost completely passivating materials, and there are no anchor points for the nucleation of dielectric materials on the surface. Perhaps the use of 2DNLMs advantages can solve this difficulty and provide a development platform in the future.

(ii) Develop new 2DLMs/2DNLMs heterojunction members

In the past decade, a large number of 2D materials with different properties have been discovered. However, so far, due to some physical properties of 2DNLMs, such as toxicity, only dozens of 2DNLMs have been experimentally achieved, which greatly increases the difficulty of its production and hinders its practical application. The research of 2DLMs/2DNLMs heterojunction mainly focuses on the application of photoelectric devices and catalysts that strongly rely on surface reactions. More research should be done to conceive and manufacture new heterostructures composed of different 2DLMs and 2DNLMs, which may produce some unexpected features and potential applications. For example, non-layered semiconductors AlGaN and GaN have shown advantages in 2D materials field such as wide band gap, high electron mobility, high carrier saturation velocity, high chemical hardness, and high radiation intensity. The addition of 2DNLMs will further expands the application prospect of 2D materials heterojunctions in high-power and biochemical sensing equipment, *etc*.

(iii) Develop material synthesis technology

From a synthesis point of view, CVD and PVD are proven as effective methods to obtain 2DNLMs, there are still some

shortcomings. Most of the obtained 2DNLMs have a processing thickness of more than 5 nm, and the growth rate is slow, and the uniformity and continuity are poor, which not only limit the research on the single-layer or few-layer materials properties, but also hinder the development of its potential applications. And the quality of the interface between 2DLMs and 2DNLMs plays a crucial role in realizing high-performance heterojunction devices. The defects in the heterostructure interface should be suppressed by adjusting the growth process and passivation treatment and so on. With the development of synthesis technology, it is also possible to design and implement more complex multilayer 2DLMs/2DNLMs heterostructures, which is of great significance to the design of multifunctional devices in the future. Therefore, the understanding of the preparation mechanism of 2DNLMs and the study of corresponding theory are necessary, which lay the foundation for the development and application of 2D materials.

2DLMs/2DNLMs vdW heterostructure is a relatively new field but exciting research field. There are more interesting properties and wider application areas waiting for us to study and develop. We believe that through more efforts, the heterostructure of 2DLMs and 2DNLMs can open up a new way for new applications with excellent performance.

Acknowledgements

Project supported by the National Natural Science Foundation of China (Grant Nos. 61731019, 60908012, 61575008, and 61775007) and the Beijing Natural Science Foundation (Grant Nos. 4182015 and 4202010). The authors are grateful for the technical support of the processing platform of the Suzhou Institute of Nano-Tech and Nano-Bionics, Chinese Academy of Sciences (SINANO). Thanks for the support of the Key Laboratory of Nanodevices and Applications, Suzhou Institute of Nano-Tech and Nano Bionics, Chinese Academy of Sciences.

References

[1] Zeng J W, Liang S J, Gao A, Wang Y, Pan C, Wu C, Liu E, Zhang L, Cao T, Liu X, Fu Y, Wang Y, Watanabe K, Taniguchi T, Lu H and Miao F 2018 *Phys. Rev. B* **98** 125414
[2] Wang F, Wang Z, Shifa T A, Wen Y, Wang F, Zhan X, Wang Q, Xu K, Huang Y, Yin L, Jiang C and He J 2017 *Adv. Funct. Mater.* **27** 1603254
[3] Cheng Y, Wang J Z, Wei X X, Guo D, Wu B, Yu L W, Wang X R and Shi Y 2015 *Chin. Phys. Lett.* **32** 117801
[4] Sun S, Dang J, Xie X, Yu Y, Yang L, Xiao S, Wu S, Peng K, Song F, Wang Y, Yang J, Qian C, Zuo Z and Xu X 2020 *Chin. Phys. Lett.* **37** 087801
[5] Wang J H, Quan Y M, Liu D Y and Zou L J 2020 *Chin. Phys. Lett.* **37** 017101
[6] Li L, Yang F, Ye G J, Zhang Z, Zhu Z, Lou W, Zhou X, Li L, Watanabe K, Taniguchi T, Chang K, Wang Y, Chen X H and Zhang Y 2016 *Nat. Nanotechnol.* **11** 593
[7] Zhang M L, Zou X M and Liu X Q 2020 *Chin. Phys. Lett.* **37** 118501
[8] Xiao R C, Wang Z, Zhang Z Q, Liu J and Jiang H 2021 *Chin. Phys. Lett.* **38** 057301
[9] Zhou S H, Zhou C W, Yang X D, Li Y, Zhong J Q and Mao H Y 2021 *Chin. Phys. Lett.* **38** 057305
[10] Zhang Y, Wang X X and Shi L J 2020 *J. Phys: Condens Matter* **33** 115301
[11] Liu J, Li X, Wang H, Yuan G, Suvorova A, Gain S, Ren Y and Lei W 2020 *ACS Appl. Mater. Interfaces* **12** 31810
[12] Zhou N, Yang R and Zhai T 2019 *Mater. Today Nano* **8** 100051
[13] Shin G H, Park C, Lee K J, Jin H J and Choi S Y 2020 *Nano Lett.* **20** 5741
[14] Murali K, Abraham N, Das S, Kallatt S and Majumdar K H 2019 *ACS Appl. Mater. Interfaces* **11** 30010
[15] Huang Z, Jiang Y, Han Q, Yang M, Han J, Wang F, Luo M, Li Q, Zhu H, Liu X, Gou J and Wang J 2020 *Nanotechnology* **31** 064001
[16] Mukherjee S, Dutta D, Mohapatra P K, Dezanashvili L, Ismach A and Koren E 2020 *ACS Nano* **14** 17543
[17] Wu Z, Jie W, Yang Z and Hao, J 2020 *Mater. Today Nano* **12** 100092
[18] Zheng Z, Yao J, Li J and Yang G 2020 *Mater. Horizons* **7** 2185
[19] Wang F, Wang Z, Wang Q, Wang F, Yin L, Xu K, Huang Y and He J 2015 *Nanotechnology* **26** 292001
[20] Wang H, Strait J H, George P A, Shivaraman S, Shields V B, Chandrashekhar M, Hwang J, Rana F, Spencer M G, Ruiz-Vargas C S and Park J 2010 *Appl. Phys. Lett.* **96** 081917
[21] Graham M W, Shi S F, Ralph D C, Park J and McEuen P L 2013 *Nat. Phys.* **9** 103
[22] Jiang X, Zhao J and Ahuja R 2013 *J. Phys: Condens. Matter* **25** 122204
[23] Li L, Wang W K, Chai Y, Li H Q, Tian M L and Zhai T Y 2017 *Adv. Funct. Mater.* **27** 1701011
[24] Bai X D, Wang E G, Yu J and Yang H 2000 *Appl. Phys. Lett.* **77** 67
[25] Li L, Yu Y, Ye G J, Ge Q, Ou X, Wu H, Feng D, Chen X H and Zhang Y 2014 *Nat. Nanotechnol.* **9** 372
[26] Xie Y, Wu E, Zhang J, Hu X, Zhang D and Liu J 2019 *ACS Appl. Mater. Interfaces* **11** 14215
[27] Xie Y, Zhang B, Wang S, Wang D, Wang A, Wang Z, Yu H, Zhang H, Chen Y, Zhao M, Huang B, Mei L and Wang J 2017 *Adv. Mater.* **29** 1605972
[28] Voiry D, Mohite A and Chhowalla M 2015 *Chem. Soc. Rev.* **44** 2702
[29] Afzaal M and O'Brien P 2006 *J. Mater. Chem.* **16** 1597
[30] Sucharitakul S, Goble N J, Kumar U R, Sankar R, Bogorad Z A, Chou F C, Chen Y T and Gao X P 2015 *Nano. Lett.* **15** 3815
[31] Zhao H, Mao Y, Mao X, Shi X, Xu C, Wang C, Zhang S and Zhou, D 2017 *Adv. Funct. Mater.* **28** 1704855
[32] Fu L, Kane C L and Mele E J 2007 *Phys. Rev. Lett.* **98** 106803
[33] Hsieh D, Qian D, Wray L, Xia Y, Hor Y S, Cava R J and Hasan M Z 2008 *Nature* **452** 970
[34] Han M, Ma J, Xu H and Liu Y 2015 *CrystEngComm* **17** 8449
[35] Chithambararaj A, Rajeswari Yogamalar N and Bose A C 2016 *Cryst. Growth Des.* **16** 1984
[36] Li W, Cheng F, Tao Z and Chen J 2006 *J. Phys. Chem. B* **110** 119
[37] Coquet R and Willock D J 2005 *Phys. Chem. Chem. Phys.* **7** 3819
[38] Gu Y Y, Wang Y F, Xia J and Meng X M 2020 *Chin. Phys. Lett.* **37** 048101
[39] Al Balushi Z Y, Wang K, Ghosh R K, Vila R A, Eichfeld S M, Caldwell J D, Qin X, Lin Y C, DeSario P A, Stone G, Subramanian S, Paul D F, Wallace R M, Datta S, Redwing J M and Robinson J A 2016 *Nat. Mater.* **15** 1166
[40] Yang M, Shu H, Tang P, Liang P, Cao D and Chen X 2013 *ACS Appl. Mater. Interfaces* **13** 8764
[41] Sun X, Shi L, Huang H, Song X and Ma T 2020 *Chem. Commun.* **56** 11000
[42] Tian Z, Wei C and Sun J 2020 *Nanoscale Adv.* **2** 2220
[43] Zhang Q, Hu Y, Guo S, Goebl Ja and Yin Y 2010 *Nano Lett.* **10** 5037
[44] Barman S K and Huda M N 2019 *Phys. Status solidi- R* **13** 1800554
[45] Kim J, Oh S, Mastro M A and Kim J 2016 *Phys. Chem. Chem. Phys.* **18** 15760
[46] Hwang W S, Verma A, Peelaers H, Protasenko V, Rouvimov S, Xing H, Seabaugh A, Haensch W, De Walle C V, Galazka Z, Albrecht M, Fornari R and Jena D 2014 *Appl. Phys. Lett.* **104** 203111
[47] Du Y, Xue Q, Zhang Z, Xia F, Li J and Han Z 2013 *Sensors Actuat B-Chem.* **186** 796
[48] Zhang C, Xu Y, Lu P, Wei C, Zhu C, Yao H, Xu F and Shi J 2019 *Angew. Chem. Int. Ed.* **58** 8814
[49] Duan H, Yan N, Yu R, Chang C R, Zhou G, Hu H S, Rong H, Niu Z, Mao J, Asakura H, Tanaka T, Dyson P J, Li J and Li Y 2014 *Nat. Commun.* **5** 1

[50] Gao S, Lin Y, Jiao X, Sun Y, Luo Q, Zhang W, Li D, Yang J and Xie Y 2016 *Nature* **529** 68
[51] Mohite S V, Ganbavle V V and Rajpure K Y 2017 *Mater. Res. Bull.* **95** 491
[52] Liu J, Lin X, Sun M, Du B, Li L, Bai J and Zhou M 2020 *Talanta* **219** 121323
[53] Lin Y, Hu H and Hu Y H 2020 *Appl. Surf. Sci.* **502** 144202
[54] Lin X, Yan P, Xu F, Wu W, Hu T, Wei C and Xu Q 2019 *J. Mater. Chem. C* **7** 7196
[55] Mohiuddin M, Zavabeti A, Haque F, Mahmood A, Datta R S, Syed N, Khan M W, Jannat A, Messalea K, Zhang B Y, Chen G, Zhang H, Ou J Z and Mahmood N 2020 *J. Mater. Chem. A* **8** 2789
[56] Wang F, Yu Y, Yin X, Tian P and Wang X 2017 *J. Mater. Chem. A* **5** 9060
[57] Feng W, Wang X, Zhang J, Wang L, Zheng W, Hu P, Cao W and Yang B 2014 *J. Mater. Chem. C* **2** 3254
[58] Wen Y, Wang Q, Yin L, Liu Q, Wang F, Wang F, Wang Z, Liu K, Xu K, HuangY, Shifa T A, Jiang C, Xiong J and He J 2016 *Adv. Mater.* **28** 8051
[59] Zhao X, Qing Y, Huang H, Yu Q, Liu B, Yang J, Dong Z, Shen Z, Zhu B and Liao L 2021 *Nano Research* **14** 1955
[60] Lu J, Zheng Z, Yao J, Gao W, Xiao Y, Zhang M and Li J 2020 *Nanoscale* **12** 7196
[61] Chu J, Zhang Y, Wen Y, Qiao R, Wu C, He P, Yin L, Cheng R, Wang F, Wang Z, Xiong J, Li Y and He J 2019 *Nano Lett.* **19** 2154
[62] Sun Y, Sun Z, Gao S, Cheng H, Liu Q, Piao J, Yao T, Wu C, Hu S, Wei S and Xie Y 2012 *Nat. Commun.* **3** 1057
[63] Wang Q, Cai K, Li J, Huang Y, Wang Z, Xu K, Wang F, Zhan X, Wang F, Wang K and He J 2016 *Adv. Mater.* **28** 617
[64] Che Y, Liu K, Liu J, Lv T, Wei B, Zhang T, Zeng M, Wang Z and Fu L 2018 *J. Am. Chem. Soc.* **140** 16392
[65] Wang D, Chen X, Fang X, Tang J, Lin F, Wang X, Liu G, Liao L, Ho J C and Wei Z 2021 *Nanoscale* **13** 1086
[66] Bai Y, Zhang H, Zhang M, Wang D, Zeng H, Zhao J, Xue H, Wu G, Su J, Xie Y, Zhang Y, Jing H, Yu H, Hu Z, Peng R, Wang M and Wu Y 2020 *Nanoscale* **12** 1100
[67] Chai R, Chen Y, Zhong M, Yang H, Yan F, Peng M, Sun Y, Wang K, Wei Z, Hu W, Liu Q, Lou Z and Shen G 2020 *J. Mater. Chem. C* **8** 6388
[68] Liu B, Wang Y, Peng H Q, Yang R, Jiang Z, Zhou X, Lee C S, Zhao H and Zhang W 2018 *Adv. Mater.* **30** 1803144
[69] Yao K, Chen P, Zhang Z, Li J, Ai R, Ma H, Zhao B, Sun G, Wu R, Tang X, Li B, Hu J, Duan X and Duan X 2018 *npj 2D Mater. Appl.* **2** 1
[70] Feng W, Zhao Y, Zhao D, Wang W, Xia Z, Zheng X, Wang X, Wang W and Wang W 2021 *RSC Adv.* **11** 3673
[71] Wilson N R, Nguyen P V, Seyler K, Rivera P, Marsden A J, Laker Z P L, Constantinescu G C, Kandyba V, Barinov A, Hine N D M, Xu X and Cobden D H 2017 *Sci. Adv.* **3** e1601832
[72] Feng W, Zheng W, Chen X, Liu G, Cao W and Hu P 2015 *Chem. Mater.* **27** 983
[73] Yang Z and Hao J 2016 *J. Mater. Chem. C* **4** 8859
[74] Zhou J 2019 *Appl. Phys. Lett.* **115** 162104
[75] Zheng Z, Yao J and Yang G 2017 *ACS Appl. Mater. Interfaces* **9** 7288
[76] Wang Q, Wen Y, He P, Yin Ll Wang Z, Wang F, Xu K, Huang Y, Wang F, Jiang C and He J 2016 *Adv. Mater.* **28** 6497
[77] Wen Y, Yin L, He P, Wang Z, Zhang X, Wang Q, Shifa T A, Xu K, Wang F, Zhan X, Wang F, Jiang C and He J 2016 *Nano Lett.* **16** 6437
[78] Balakrishnan N, Kudrynskyi Z R, Smith E F, Fay M W, Makarovsky O, Kovalyuk Z D, Eaves L, Beton P H and PatanèA 2017 *2D Mater.* **4** 025043
[79] Ren D, Merdrignac-Conanec O, Dorcet V, Cathelinaud M, Zheng Z, Ma H and Zhang X 2020 *Ceram. Int.* **46** 25503
[80] Kim S, Oh S and Kim J 2019 *ACS Photon.* **6** 1026
[81] Yan X, Esqueda I S, Ma J, Tice J and Wang H 2018 *Appl. Phys. Lett.* **112** 032101
[82] Kim J, Mastro M A, Tadjer M J and Kim J 2018 *ACS Appl. Mater. Interfaces* **10** 29724
[83] Kim J, Mastro M A, Tadjer M J and Kim J 2017 *ACS Appl. Mater. Interfaces* **9** 21322
[84] Puthirath Balan A, Radhakrishnan S, Woellner C F, Sinha S K, Deng L, Reyes C D L, Rao B M, Paulose M, Neupane R, Apte A, Kochat V, Vajtai R, Harutyunyan A R, Chu C W, Costin G, Galvao D S, Martí A A, Van Aken P A, Varghese O K, Tiwary C S, Malie Madom Ramaswamy Iyer A and Ajayan P M 2018 *Nat. Nanotechnol.* **13** 602
[85] Kim J and Kim J 2020 *ACS Appl. Mater. Interfaces* **12** 7310
[86] Zhuo R, Wu D, Wang Y, Wu E, Jia C, Shi Z, Xu T, Tian Y and Li X 2018 *J. Mater. Chem. C* **6** 10982
[87] Kong W Y, Wu G A, Wang K Y, Zhang T F, Zou Y F, Wang D D and Luo L B 2016 *Adv. Mater.* **28** 10725
[88] Chemelewski W D, Lee H C, Lin J F, Bard A J and Mullins C B 2014 *J. Am. Chem. Soc* **136** 2843
[89] Kalita G, Mahyavanshi R D, Desai P, Ranade A K, Kondo M, Dewa, T and Tanemura M 2018 *Phys. Status Solidi-R* **12** 1800198
[90] Zhou N, Gan L, Yang R, Wang F, Li L, Chen Y, Li D and Zhai T 2019 *ACS Nano* **13** 6297
[91] Lu J, Zheng Z, Gao W, Yao J, Zhao Y, Xiao Y, Wang B and Li J 2019 *J. Mater. Chem. C* **7** 12104
[92] Zhu D D, Xia J, Wang L, Li X Z, Tian L F and Meng X M 2016 *Nanoscale* **8** 11375
[93] Wang Q, Xu K, Wang Z, Wang F, Huang Y, Safdar M, Zhan X, Wang F, Cheng Z and He J 2015 *Nano Lett.* **15** 1183
[94] Wang Q, Wang F, Li J, Wang Z, Zhan X and He J 2015 *Small* **11** 4613
[95] Zheng W, Feng W, Zhang X, Chen X, Liu G, Qiu Y, Hasan T, Tan P and Hu P A 2016 *Adv. Funct. Mater.* **26** 2648
[96] Schornbaum J, Winter B, Schießl S P, Gannott F, Katsukis G, Guldi D M, Spiecker E and Zaumseil J 2014 *Adv. Funct. Mater.* **24** 5798
[97] Wang Q, Wen Y, Yao F, Huang Y, Wang Z, Li M, Zhan X, Xu K, Wang F, Wang F, Li J, Liu K, Jiang C, Liu F and He J 2015 *Small* **11** 5388
[98] Cheng R, Wen Y, Yin L, Wang F, Wang F, Liu K, Shifa T A, Li J, Jiang C, Wang Z and He J 2017 *Adv. Mater.* **29** 1703122
[99] Zhu D D, Xia J, Wang L, Li X Z, Tian L F and Meng X M 2016 *Nanoscale* **8** 11375
[100] Wang Y, Yang Z, Li H, Li S, Zhi Y, Yan Z, Huang X, Wei X, Tang W and Wu Z 2020 *ACS Appl. Mater. Interfaces* **12** 47714
[101] Jiang W, Zheng T, Wu B, Jiao H, Wang X, Chen Y, Zhang X, Peng M, Wang H, Lin T, Shen H, Ge J, Hu W, Xu X, Meng X, Chu J and Wang J 2020 *Light: Sci. Appl.* **9** 1
[102] Oliva N, Casu E A, Yan C, Krammer A, Rosca T, Magrez A, Stolichnov I, Schueler A, Martin O J F and Ionescu A M 2017 *ACS Appl. Mater. Interfaces* **9** 26325
[103] Zhang X, Li J, Ma Z, Zhang J, Leng B and Liu B 2020 *ACS Appl. Mater. Interfaces* **12** 47721
[104] Lu J, Wei A, Zhao Y, Tao L, Yang Y, Zheng Z, Wang H, Luo D, Liu J, Tao L, Li H, Li J and Xu J B 2018 *ACS Photon.* **5** 4912
[105] Lu J, Zheng Z, Yao J, Gao W, Zhao Y, Xiao Y and Li J 2019 *Small* **15** 1904912
[106] Yadava N and Chauhan R K 2019 *ECS J. Solid State Sci. Technol.* **8** Q3058
[107] Choi W, Ahn J, Kim K T, Jin H J, Hong S, Hwang D K and Im S 2021 *Adv. Mater.* **2021** e2103079
[108] Lei M Y, Liu C M, Zhou Y G, Yan Z H, Han S B, Liu W, Xiang X and Zu X T 2016 *Chin. J. Phys.* **54** 51
[109] Su B, He H and Ye Z 2019 *Mater. Lett.* **253** 187
[110] Weng J and Gao S P 2019 *RSC Adv.* **9** 32984
[111] Zhou J, Xie M, Ji H, Cui A, Ye Y, Jiang K, Shang L, Zhang J, Hu Z and Chu J 2020 *ACS Appl. Mater. Interfaces* **12** 18674
[112] Bi K, Wan Q, Shu Z, Shao G, Jin Y, Zhu M, Lin J, Liu H, Liu H, Chen Y, Liu S, Duan H 2020 *Sci. China Mater.* **63** 1076
[113] Oh S, Kim C K and Kim J 2018 *ACS Photon.* **5** 1123
[114] Liu Z, You L, Faraji N, Lin C H, Xu X, He J H, Seidel J and Wang J 2020 *Adv. Funct. Mater.* **30** 1909672
[115] Zhang X, Zhang Z, Liang J, Zhou Y, Tong Y, Wang Y and Wang X 2017 *J. Mater. Chem. A* **5** 9702
[116] Zhao S, Wang Y, Zhang Q, Li Y, Gu L, Dai Z, Liu S, Lan Y Q, Han M and Bao J 2016 *Inorg. Chem. Front.* **3** 1501
[117] Yang Q, Tan C J, Meng R S, Jiang J K, Liang Q H, Sun X, Yang D G and Chen X 2017 *IEEE Electron Dev. Lett.* **38** 145
[118] Yang Q, Zhang S, Tan C, Ye H, Ming X, Ingebrandt S and Chen X 2017 *J. Mater. Chem. C* **5** 9412
[119] Kumar S, Maivizhikannan V, Drews J and Krishnan V 2019 *Vacuum* **163** 88
[120] Rahimi K, Moradi M, Dehghan R and Yazdani A 2019 *Mater. Lett.* **234** 134
[121] Selvaraj R, Kalimuthu K R and Kalimuthu V 2019 *Mater. Lett.* **243** 183
[122] Chen J, Wu X J, Lu Q, Zhao M, Yin P F, Ma Q, Nam G H, Li B, Chen B and Zhang H 2021 *Small* **17** 2006135
[123] Mojaddami M and Simchi A 2020 *Renew. Energ.* **162** 504
[124] Harish S, Prachi, Archana J, Navaneethan M, Shimomura M, Ikeda H and Hayakawa Y 2019 *Appl. Surf. Sci.* **488** 36